공학박사 학위논문

Light Olefins Production through Catalytic Cracking of C_5 Raffinate over Modified ZSM-5 Catalyst

변형된 ZSM-5 촉매 상에서 C_5 라피네이트의 촉매접촉분해를 통한 경질올레핀 제조

2014년 8월

서울대학교 대학원

화학생물공학부

이 중 원

Abstract

Light Olefins Production through Catalytic Cracking of C_5 Raffinate over Modified ZSM-5 Catalyst

Joongwon Lee

School of Chemical and Biological Engineering

The Graduate School

Seoul National University

Light olefins, such as ethylene and propylene, are important materials of petrochemical industry, and they are mostly used to produce various chemicals and polymers. Currently, light olefins are mainly produced by thermal cracking of naphtha. However, thermal cracking is generally carried out at high reaction temperature (over 800 ^{o}C). Furthermore, thermal cracking process has a limitation to control product distribution. Catalytic cracking has been considered as the effective method to produce light olefins due to its prominent ability to reduce reaction temperature and its easiness to control product distribution. Various hydrocarbons including naphtha, heavy oil, and C_4/C_5 hydrocarbons have been used to produce light olefins. Among them, C_5 raffinate, which is produced as a by-product in the naphtha cracking center,

has been considered as a promising feedstock to produce light olefins.

ZSM-5 has been considered as an effective catalyst in the production of light olefins through catalytic cracking of light hydrocarbons due to its unique structure and intrinsic activity. However, microporous feature of ZSM-5 strongly affects the mass transfer of reaction species, which restricts the catalytic conversion. Furthermore, poor hydrothermal stability of ZSM-5 under the severe reaction condition caused loss of considerable amount of acid sites by dealumination, resulting in poor catalytic performance. Therefore, developing an efficient ZSM-5 catalyst with high activity and hydrothermal stability is required for the maximum light olefin production by catalytic cracking of C_5 raffiinate. In this work, a number of modified ZSM-5 catalysts, including micro/mesoporous featured ZSM-5, phosphorous modified ZSM-5, and lanthanum containing ZSM-5, were prepared for use in the production of light olefins through catalytic cracking of C_5 raffiinate.

ZSM-5 catalysts (PAM(X)-ZSM5) with micropores and mesopores were prepared using polyacrylamide (PAM) as a soft template at different PAM content (X=0, 0.12, 0.25, 0.53, 0.64, and 0.78 wt%) with an aim of accelerating the diffusion rate of reactants and reaction intermediates. The prepared catalysts were then applied to the production of light olefins (ethylene and propylene) through catalytic cracking of C_5 raffinate. The effect of PAM content of PAM(X)-ZSM5 catalysts on the physicochemical properties and catalytic activities was investigated. N_2 adsorption-desorption isotherms of PAM(X)-ZSM5 catalysts exhibited a broad hysteresis loop at high relative pressure, indicating the existence of mesopores in the catalysts. It was found that the catalytic performance of PAM(X)-ZSM5 catalysts was

closely related to the mesoporosity of the catalysts. Conversion of C_5 raffinate and yield for light olefins showed volcano-shaped trends with respect to mesopore/micropore volume ratio of the catalysts. Thus, an optimal PAM content was required to achieve maximum production of light olefins through catalytic cracking of C_5 raffinate over microporous and mesoporous PAM(X)-ZSM5 catalysts.

Microporous and mesoporous ZSM-5 (C(X)-ZSM-5) catalysts were also prepared by hard templating method using carbon as a hard template with a variation of carbon template content (X=0, 10, 20, 30, 40, and 50 wt%). The prepared catalysts were applied to the production of light olefins (ethylene and propylene) through catalytic cracking of C_5 raffinate. The effect of carbon template content on the physicochemical properties and catalytic activity of C(X)-ZSM-5 catalysts was investigated. It was revealed that physicochemical properties of C(X)-ZSM-5 catalysts were strongly influenced by carbon template content. Adsorption ability for n-pentane and mesopore volume of C(X)-ZSM-5 catalysts increased with increasing carbon template content. It was also found that catalytic performance of C(X)-ZSM-5 catalysts was closely related to the mesoporosity of the catalyst. Conversion of C_5 raffinate and yield for light olefins increased with increasing mesopore/micropore volume ratio of the catalyst, while selectivity for ethylene and propylene showed constant values. Thus, carbon template content in the C(X)-ZSM-5 catalysts strongly affected the mesoporosity of the catalyst, and in turn, mesoporosity played an important role in determining the catalytic performance in the production of light olefins through catalytic cracking of C_5 raffinate.

In order to enhance the hydrothermal stability of micro/mesoporous ZSM-5 (C-ZSM-5) catalysts prepared by carbon templating method, phosphorous modification was carried out. The phosphorous-modified microporous and mesoporous ZSM-5 catalysts (XP/C-ZSM5) were prepared with a variation of phosphorous content (X=0.17, 0.3, 0.7, 1.4, and 2.7 wt%), and they were applied to the production of light olefins through catalytic cracking of C_5 raffinate. The acidity of C-ZSM5 catalysts significantly decreased after hydrothermal treatment caused by dealumination of C-ZSM5 catalyst during the hydrothermal treatment. On the other hand, phosphorous-modified XP/C-ZSM5 reserved extended amount of acid sites after hydrothermal treatment, because phosphorous introduced in C-ZSM5 catalyst inhibited the dealumination of the catalyst. Both conversion of C_5 raffinate and yield for light olefins showed volcano-shaped trend with respect to phosphorous content. Among the hydrothermal treated catalysts (XP/C-ZSM5-St.) tested, 0.3P/C-ZSM5-St. catalyst showed the best catalytic performance. This result indicates that phosphorous modification of ZSM-5 can serve as an efficient method to improve the hydrothermal stability of the catalyst, and in turn, optimal phosphorous content was required for maximum production of light olefins.

Lanthanum-containing phosphorous-modified porous ZSM-5 catalysts (LaX-P/C-ZSM5) were prepared with a variation of La/Al atomic ratio (X=0.3, 0.7, 0.9, and 1.2) to obtaining a high light olefin production by suppressing secondary reaction between reactants and reaction intermediates. The prepared catalysts were then applied in the production of light olefins through catalytic cracking of C_5 raffinate. The effect of lanthanum content of

LaX-P/C-ZSM5 catalysts on their physicochemical properties and catalytic activities for the cracking of C_5 raffinate was investigated. The acidity of LaX-P/C-ZSM5 catalysts decreased with increasing lanthanum content, while basicity of LaX-P/C-ZSM5 catalysts increased with increasing lanthanum content. In the catalytic cracking of C_5 raffinate, acid and base properties of LaX-P/C-ZSM5 catalysts were closely related to the conversion of C_5 raffinate and selectivity for light olefins, respectively. Conversion of C_5 raffinate decreased with decreasing acidity of the catalyst and selectivity for light olefins increased with increasing basicity of the catalyst. Among the catalysts tested, La0.7-P/C-ZSM5 catalyst with moderate acidity and basicity exhibited the best catalytic performance in terms of yield for light olefins. It is concluded that an optimal lanthanum content of LaX-P/C-ZSM5 catalysts was required for maximum light olefin production in the catalytic cracking of C_5 raffinate.

In summary, a number of modified ZSM-5 catalysts were prepared including micro/mesoporous featured ZSM-5, phosphorous modified ZSM-5, and lanthanum containing ZSM-5, and they were applied to the production of light olefins through catalytic cracking of C_5 raffiinate. Various experimental measurements such as BET, NH_3-TPD, CO_2-TPD, and n-pentane TPD analyses were carried out to elucidate the catalytic performance of modified ZSM-5 catalysts. It was revealed that textural property and acid-base property of the catalyst played a crucial role in determining the catalytic performance in the catalytic cracking of C_5 raffinate to light olefins.

Keywords: ZSM-5 zeolite, Light olefins, C_5 raffinate, Acidity, Basicity,

Catalytic cracking

Student Number: 2011-30280

Contents

List of Tables

List of Figures

Chapter 1. Introduction

1.1. Light olefins

Light olefins, such as ethylene and propylene, is one of the key building block petrochemicals and are mostly used to produce plastics, fibers, and other chemicals [1,2]. The demand for ethylene and propylene in the market reaches 120 million tons/yea and 70 million tons/year, respectively. The market demand for light olefins will continue to grow at 4-5% annually, and average growth rate of propylene will be about 1% higher than that of ethylene [3]. This trend will continue for the next 10 years and the shortage of propylene supply will not be covered only by the current propylene production process (thermal cracking of naphtha).

The main commercial technique for light olefins production is steam cracking of hydrocarbons. The yield for ethylene and propylene varies between 24-55% and 1.5-18%, respectively depending greatly on the feedstock type and operating condition [4-6]. Steam cracking is the most energy-consuming process in petrochemical industry even though various improvements have been made in this process such as modification of cracking furnace (radiant tube and coils) and introduction of heat recovery systems. However, marginal technological improvements cannot make further improvement in energy efficiency. The current steam cracking process uses as much as 40% of the energy consumed by the entire petrochemical industry, and results in high amount of CO_2 emission [7]. Furthermore, stream cracking

has limit to control P/E (propylene to ethylene) ratios coming from the steam cracker, and it directly dependence on the type of feedstock [1,4,8]. Hence, there is an increasing demand for processes capable of controlling the composition of olefins.

1.2. Technologies for light olefins production

A number of technologies, such as and catalytic cracking [9-11], metathesis of ethylene and 2-butene [12,13], MTO (methanol to olefin) [14-16], direct or oxidative dehydrogenation of ethane and propane [17-19], and oxidative coupling of methane have been proposed for the production of light olefins [20,21]. Among these technologies, catalytic cracking of hydrocarbon has been recognized the most effective method to produce light olefins.

Majority of light olefin production today is produced by catalytic cracking process due to its prominent ability to reduce reaction temperature and its easiness to control product distribution. As shown in Fig. 1.2, catalytic cracking technology can save activation energy use in conventional steam cracking [5]. Thus catalytic cracking can be carried out at moderate temperature and pressure in comparison with steam cracking. Furthermore, catalytic cracking process improves selectivity to desired product according to the market demand [1]. Coke formed during the cracking process is constantly removed by catalysts that are in turn decoked through catalyst regeneration or catalyst decoking. Although conventional naphtha has been employed as main feedstock of light olefin production, uses of alternative feedstocks such as methane, LPG, gas oil, crude oil, and ethanol have also been pursued.

$$C_2H_4 + C_4H_8 \rightarrow 2C_3H_6 \qquad (1.1)$$

Olefin metathesis, first reported in the 1960s, is an alternative process

of steam cracking because it can convert a mixture of ethylene and 2-butene into the more valuable propylene with flexibility according to the economic climate [22]. The Phillips triolefin process, which utilizes a heterogeneous catalyst system, was originally developed by Phillips Petroleum Co., USA, and operated from 1966 to 1972 for the conversion of propylene into ethylene and 2-butene, due to less propylene demand at that time [12]. The metathesis reaction take place in fixed-bed reactor at higher than 260 ^{o}C and 30-35 bar over mixture of WO_3/SiO_2 and MgO catalysts. The conversion of 2-butene is above 60% per mass and the selectivity for propylene is higher that 90% [23,24]. It is well demonstrated that olefin metathesis has potential application for producing propylene in a large scale for the petrochemical industry. In particular, naphtha steam crackers with an integrated metathesis unit are an interesting alternative for the production of propylene.

$$2CH_3OH \overset{H_2O}{\leftrightarrow} CH_3OCH_3 \overset{H_2O}{\rightarrow} C_2\text{-}C_5 \text{ olefins} \rightarrow \text{iso-paraffins} + \text{aromatics} \qquad (1.2)$$

The development of shale gas has decreased the price of natural gas and has renewed interest in transforming methane into alcohol such as methanol and ethanol that can be used for the production of clean fuel and chemicals [25]. Mobil's zeolite based process for the conversion of methanol to gasoline provided a new route for the conversion of coal to gasoline. The importance of light olefins as intermediates in the conversion of methanol to gasoline has prompted several studies on methods for selectively producing them from methanol on zeolite catalysts [16]. As shown in reaction scheme, methanol is

first dehydrated to dimethylether (DMC). The equilibrium mixture of methanol, DME, and water is then converted to light olefins. In the final step other higher olefins, iso-paraffins, and aromatics are produced. Zeolite based catalyst such as ZSM-5 and SAPO-34 is being generally used for the conversion of methanol into olefins [16,26,27].

$$2C_2H_6 \text{ or } 2C_3H_8 + O_2 \rightarrow 2C_2H_4 \text{ or } 2C_3H_6 + 2H_2O \quad (1.3)$$

Many efforts have been made to chemical conversion of light alkanes to valuable chemicals. In particular, the increased demand for light olefins required the development and understanding of new catalytic routes to produce light olefins from light alkanes [18]. Thus, direct dehydrogenation and oxidative dehydrogenation of ethane and propane were proposed to produce ethylene and propylene [28]. Compared with direct dehydrogenation reaction, oxidative dehydrogenation reaction is more preferred to produce light olefins from ethane and propane, because the presence of oxygen raises the thermodynamic restrictions of dehydrogenation and the exothermic character of reaction increase the energy efficiency. The high activity and selectivity for light olefins are shown by metal oxide catalysts either on vanadium base (V-Sb, V-P, V-Mo) or on molybdenum base (Mo-Ni, Mo-Co) [29,30].

$$CH_4 + O_2 \rightarrow C_2H_6 + H_2O \rightarrow C_2H_4 + \text{others} \quad (1.4)$$

Methane, a principal component of natural gas, is an abundant

hydrocarbon resource that is mainly used as a relatively inexpensive and clean-burning fuel [20]. The oxidative coupling of methane (OCM) to ethylene is an attractive alternative for the stream cracking of naphtha. The large number of different catalyst has been investigated, such as Li/MgO, La_2O_3, Ba/MgO, and $NaMnO_4$/MgO catalysts, for the OCM reaction [31-33]. However, OCM reaction has several problems. When the reaction temperature is lower than 600 ^oC, rate of reaction is slow, but above 600 ^oC undesired oxidations dominate the reaction. Thus, low yield for ethylene is obtained.

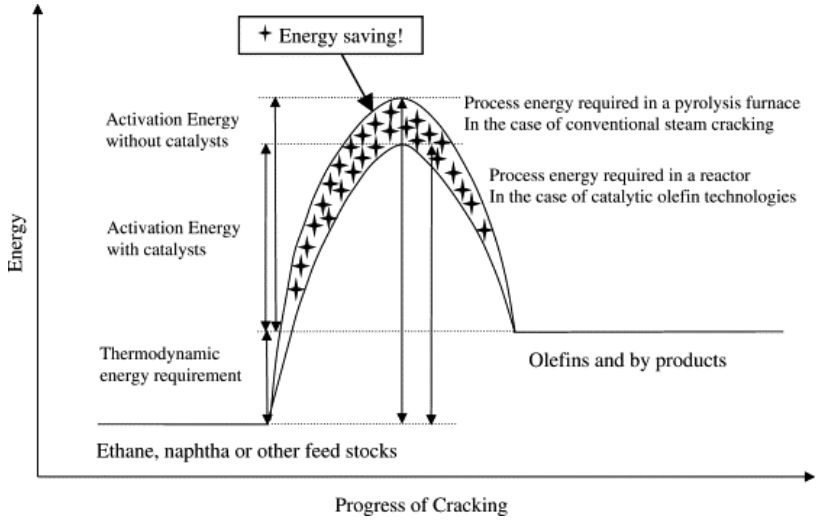

Fig. 1.1. Energy profile of conventional steam cracking and catalytic cracking [5].

1.3. Catalytic cracking catalyst

Various types of catalysts (basic catalysts, transition metal oxide catalysts, and acid catalysts) have been studied in the catalytic cracking of hydrocarbons to achieve higher yield of light olefins [7]. The catalytic performance and reaction conditions in the catalytic cracking of naphtha to light olefins depending on the types of catalyst are listed in Table 1.1.

Catalytic cracking over basic catalysts such as CaO-SrO-Al_2O_3, WO_3-K_2O-Al_2O_3, and KVO_3/corundum with steam condition is believed to follow a free radical mechanism [34-36]. Compared with the conventional steam cracking, the yield for ethylene from naphtha was increased 5-10%, at 770-820 ^oC. However, high reaction temperature (770-820 ^oC) and high feed-rate of steam decrease the energy efficiency of light olefin production from naphtha.

Transition metal oxide catalysts were expected to promote oxidative cracking of hydrocarbons by supplying the activation energy via internal combustion of hydrocarbons [37,38]. Another expectation was that these catalysts, such as Na/P/Mn/SiO_2 catalysts, could be used in fluid catalytic cracking (FCC) type unit, where lattice oxygen is mainly used for oxidative cracking in the reactor and the partly reduced catalysts are re-oxidized in to regenerator. Among transition metal oxide catalysts, V-oxides are known to show an oxidative dehydrogenation function for alkane activation in the presence of oxygen at low temperature. Although high yield for ethylene can be obtained using transition metal oxide catalyst, the precise control of

combustion reactions is necessary. In general, the advantages of oxidative catalytic cracking are to shift the equilibrium and to lower reaction temperature due to partial supply of heat by combustion reaction.

The most active and widely investigated catalysts for hydrocarbon cracking are solid acid catalysts, including zeolites, which are the key components of industrial petroleum cracking catalysts [39]. Zeolite-based acid catalysts such as ZSM-5, ZSM-23, BEA, and MCM-22 have been widely investigated as catalysts for catalytic cracking of hydrocarbons [40-44]. In particular, ZSM-5 has been considered as an effective catalyst in the production of light olefins through catalytic cracking of light hydrocarbons.

Table 1.1

The catalytic performance and reaction conditions in the catalytic cracking of naphtha to light olefins depending on the types of catalyst [7]

Type of catalyst	Acid catalysts	Basic catalysts	Transition metal oxide catalysts
Reaction Temperature (^{o}C)	550-650	750-850	500-800
Steam/Feed Ratio	0-1	1-2	0.5-1
Yield for Products (wt%)			
Ethylene	15-27	30-40	20-50
Propylene	15-50	15-22	3-10
Aromatics	11-34	0	-
CO, CO2	Neg.	5-20	15-30
Example of Catalysts	Ag-MOR/Al_2O_3 Cu/HZSM-5 Steamed HZSM-5	CaO-SrO-Al_2O_3 WO_3-K_2O-Al_2O_3 KVO_3/corundum	Cr_2O_3/Al_2O_3 Li/MgO

1.4. ZSM-5 zeolite

ZSM-5 is a synthetic high-silica zeolite (Si/Al ratio > 7) first reported in 1973 by Argauer and Landolt. As shown in Fig. 1.2, ZSM-5 structure is described as a combination of two interconnected channel systems [45]. The silicate framework forms sinusoidal 10-member-ring (MR) channels along the direction of *a*-axis, interconnected with 10-MR straight channels that run down the *b*-axis. Because of ZSM-5's unique structure with good catalytic activity and shape selectivity, it was applied in petrochemical processing, fine chemical production, and liquid and gas separation [46]. In particular, ZSM-5 exhibited outstanding catalytic performance in catalytic cracking of hydrocarbons [42].

Many efforts have been made to enhance the catalytic performance of ZSM-5 in the production of light olefins through catalytic cracking of hydrocarbons. ZSM-5 is readily deactivated by coke formation under severe reaction conditions, resulting in a loss of catalytic activity [47]. Therefore, it is necessary to overcome such a limitation in the catalytic cracking of hydrocarbons over ZSM-5. It has been reported that addition of appropriate amount of steam into the feedstock can reduce the coke formation on ZSM-5 [48]. Furthermore, addition of second metals such as Mn and Zn into ZSM-5 has also been found to be an effective method to improve the stability of ZSM-5 [49]. Modification of ZSM-5 with phosphorous, however, has been considered as the most effective method to enhance the stability of ZSM-5 [50,51].

The small pore size of (< 1 nm) of ZSM-5 leads to diffusion limitation for bulky hydrocarbon molecules, resulting in pore blockage and coke formation. Therefore, several methods such as preparation of small ZSM-5 particles, post-treatment to create extra-porosity, and direct synthesis of mesoporous ZSM-5 have been proposed to overcome diffusion limitation [52-55]. In particular, direct synthesis of mesoporous ZSM-5 is one of the promising strategies to minimize the diffusion limitation. It has been reported that diffusion of iso-butane can be enhanced over mesoporous ZSM-5 compared to the conventional ZSM-5, although iso-butane is smaller than the pore size of ZSM-5 [56]. It was revealed that diffusivity of iso-butane over mesoporous ZSM-5 was about three times larger than that over the conventional ZSM-5. During the catalytic cracking reaction, furthermore, paraffins and adsorbed carbenium ions are oligomerized through bimolecular cracking mechanism to form large hydrocarbons. These molecules can cause pore block and diffusion limitation of ZSM-5. Therefore, it is expected that mesoporous feature of ZSM-5 can be an important factor determining the catalytic performance in the catalytic cracking of C_5 hydrocarbons. Mesoporous ZSM-5 can be synthesized using hard template or supramolecular soft template [59]. Many efforts have been made to synthesize mesoporous ZSM-5 by a carbon templating method, because carbon is easy to handle and inexpensive compared to the other templates [57,58]. Mesoporous ZSM-5 prepared by a carbon templating method has advantages in controlling mesopore diameter and pore volume by choosing suitable carbon source. For this reason, various reactions such as isomerization of hydrocarbon, alkylation of benzene, and decomposition of NO have been conducted over mesoporous

ZSM-5 prepared by a carbon templating method [59-61].

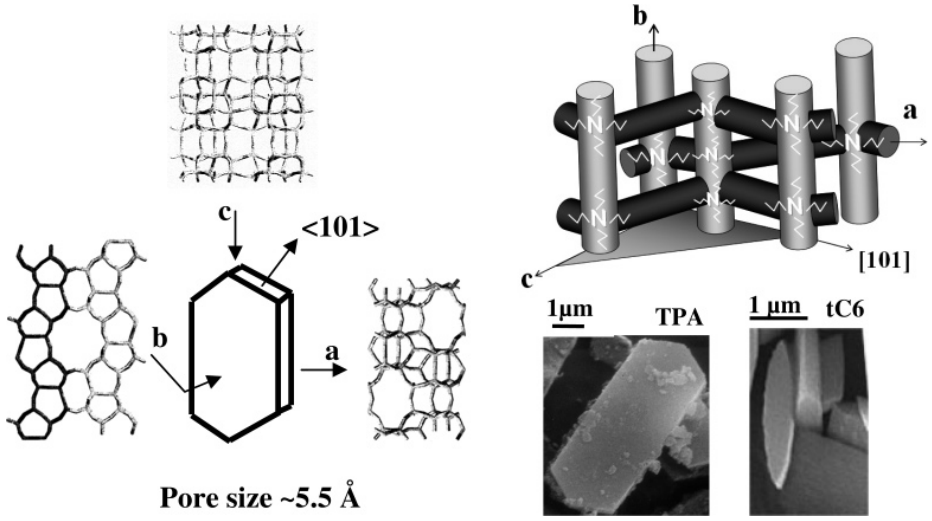

Fig. 1.2. Structure of ZSM-5 zeolite [45].

1.5. C_5 raffinate

C_5 raffinate is a residue obtained after separation of isoprene and piperylene from the C_5 raffinate stream in a naphtha cracking unit. The C_5 raffinate, therefore, is mainly composed of pentane, isopentane, pentene, isopentene, and cyclopentane. It is expected that the commercial value of C_5 raffinate can be much enhanced if light olefins is produced using C_5 raffinate as a source of feedstock through catalytic cracking of C_5 raffinate. Therefore, developing an efficient catalyst for catalytic cracking of C_5 raffinate to light olefins would be a challenging work.

Chapter 2. Experimental

2.1. Preparation of catalysts

2.1.1. Micro/mesoporous ZSM-5 catalysts prepared by soft templating method

ZSM5 catalysts (PAM(X)-ZSM5) with micropores and mesopores were prepared using polyacrylamide (PAM) as a soft template at different PAM content (X=0, 0.12, 0.25, 0.53, 0.64, and 0.78 wt%) as presented in Fig. 2.1. Molar composition of Si:Al:Na_2O:TPABr:H_2O was fixed at 1:0.03:0.07:0.03:35. Typical procedures for the preparation of PAM-templating ZSM5 catalyst are as follows. An appropriate amount of sodium hydroxide (NaOH, Samchun Chem.) was dissolved in distilled water at 40 ^oC. Known amounts of tetrapropylammonium bromide (TPABr, Sigma-Aldrich) and tetraethylorthosilicate (TEOS, Sigma-Aldrich) were added into the sodium hydroxide solution under vigorous stirring, and the mixture was stirred until a homogeneous solution was obtained (Solution A). A known amount of sodium aluminate ($NaAlO_2$, Junsei) was separately dissolved in distilled water (Solution B). Solution B was then added into Solution A. After stirring the solution at 40 ^oC for 3 h, a known amount of polyacrylamide (PAM, Sigma-Aldrich) was added under stirring for additional 3 h. The resulting mixture was put into a Teflon-lined autoclave, and crystallization

was then done at 160 ^{o}C for 72 h under autogenous pressure. After crystallization, the resultant was filtered and washed with distilled water several times to obtain a solid product. The solid product was dried overnight at 110 ^{o}C, and it was finally calcined at 650 ^{o}C for 5 h in an air stream to remove the organic template. The prepared PAM-templating ZSM5 catalysts were denoted as PAM(X)-ZSM5, where X represented wt% of PAM with respect to silicon source. For comparison, conventional pure ZSM5 was also synthesized. The preparation procedures for pure ZSM5 were identical to those for PAM-templating ZSM5, except that PAM was not employed as a template. The conventional pure ZSM5 was denoted as PAM(0)-ZSM5. All the prepared catalysts were ion-exchanged three times with 1 M solution of ammonium nitrate (NH_4NO_3, Junsei) at 80 ^{o}C for 3 h. The ion-exchanged catalyst was finally calcined at 650 ^{o}C for 5 h to obtain H-form.

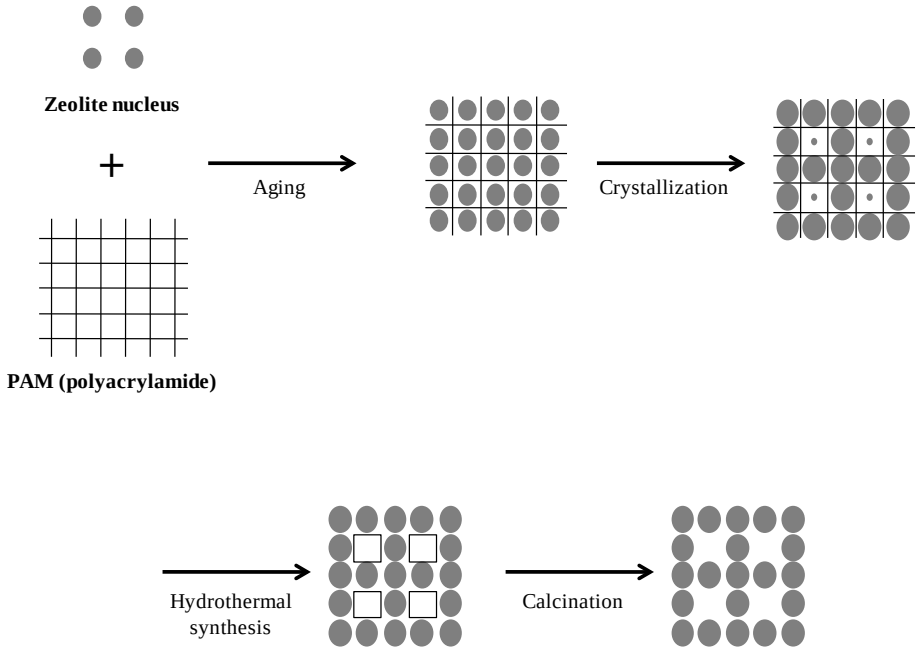

Fig. 2.1. Schematic procedures for the preparation of micro/mesoporous ZSM-5 catalysts by PAM-templating method.

2.1.2. Micro/mesoporous ZSM-5 catalysts prepared by hard templating method

ZSM-5 catalysts (C(X)-ZSM-5) with micropores and mesopores were prepared by a hard templating method using carbon as a hard template with a variation of carbon template content (X=0, 10, 20, 30, 40, and 50 wt%) as presented in Fig. 2.2. Molar composition of $Si:Al:Na_2O:TPABr:H_2O$ was fixed at 1:0.03:0.07:0.03:35. Typical procedures for the preparation of carbon-templated ZSM-5 catalyst are as follows. An appropriate amount of sodium hydroxide (NaOH, Samchun Chem.) was dissolved in distilled water at 40 ^oC. Tetrapropylammonium bromide (TPABr, Sigma-Aldrich) and colloidal silica (Ludox HS-40, Sigma-Aldrich) were added into the sodium hydroxide solution under vigorous stirring, and the mixture was stirred until a homogeneous solution was obtained (Solution A). A known amount of sodium aluminate ($NaAlO_2$, Junsei) was separately dissolved in distilled water (Solution B). Solution B was then added into Solution A. After stirring the solution at 40 ^oC for 3 h, an appropriate amount of carbon (BP2000, Carbot Corp.) was added under stirring for another 3 h. Physical properties of carbon template were listed in Table 2.1 [57]. The resulting mixture was put into a Teflon-lined autoclave, and crystallization was then carried out at 160 ^oC for 72 h under autogenous pressure. After crystallization, the resultant was filtered and washed with distilled water several times to obtain solid product. The solid product was dried overnight at 110 ^oC, and it was finally calcined at 650 ^oC for 10 h in an air stream to remove carbon and organic templates. The

prepared carbon-templated ZSM-5 catalysts were denoted as C(X)-ZSM-5, where X represented wt% of carbon template with respect to silica source.

For comparison, conventional pure ZSM-5 was also synthesized. The preparation procedures for pure ZSM-5 were identical to those for carbon-templated ZSM-5, except that carbon was not employed as a secondary template. The conventional pure ZSM-5 was denoted as C(0)-ZSM-5. Since the prepared catalyst retained Na-form, each catalyst was ion-exchanged three times with 1 M solution of ammonium nitrate (NH_4NO_3, Junsei) at 80 ^oC for 3 h. The ion-exchanged catalyst was finally calcined at 650 ^oC for 5 h to obtain H-form.

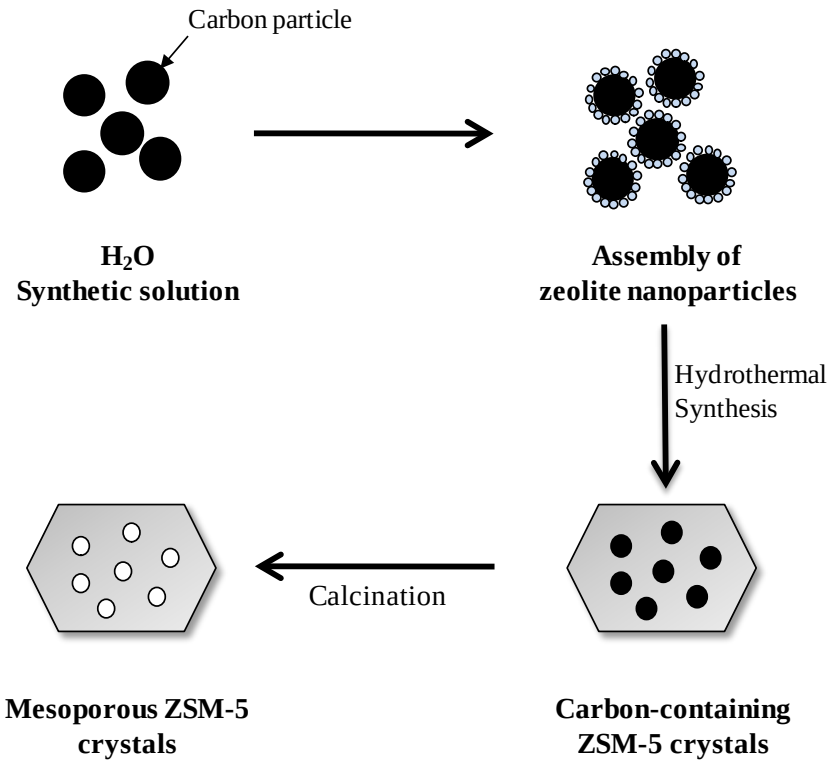

Fig. 2.2. Schematic procedures for the preparation of micro/mesoporous ZSM-5 catalysts by carbon-templating method.

Table 2.1

Physical properties of carbon template

Carbon template	BP2000
BET surface area (m^2/g)	1500
Primary particle size (nm)	12
Bulk density (g/cm^3)	0.15

2.1.3. Phosphorous modified micro/mesoporous ZSM-5 catalysts

The microporous and mesoporous ZSM-5 catalyst was prepared by a carbon-templating method. Molar composition of Si:Al:Na_2O:TPABr:H_2O was fixed at 1:0.03:0.07:0.03:35. Typical procedures for the preparation of carbon-templated ZSM-5 catalyst are as follows. An appropriate amount of sodium hydroxide (NaOH, Samchun Chem.) was dissolved in distilled water at 40 ^{o}C. Tetrapropylammonium bromide (TPABr, Sigma-Aldrich) and colloidal silica (Ludox HS-40, Sigma-Aldrich) were added into the sodium hydroxide solution under vigorous stirring, and the mixture was stirred until a homogeneous solution was obtained (Solution A). A known amount of sodium aluminate ($NaAlO_2$, Junsei) was separately dissolved in distilled water (Solution B). Solution B was then added into Solution A. After stirring the solution at 40 ^{o}C for 3 h, carbon template (BP2000, Carbot Corp.) was added under stirring for additional 3 h. The amount of carbon template introduced into the solution was 30 wt% with respect to silica source. The resulting mixture was put into a Teflon-lined autoclave, and crystallization was then carried out at 160 ^{o}C for 72 h under autogenous pressure. After crystallization, the resultant was filtered and washed with distilled water several times to obtain solid product. The solid product was dried overnight at 110 ^{o}C, and it was finally calcined at 650 ^{o}C for 10 h in an air stream to remove carbon and organic templates. The catalyst was ion-exchanged three times with 1 M solution of ammonium nitrate (NH_4NO_3, Junsei) at 80 ^{o}C for 3 h. The ion-exchanged catalyst was finally calcined at 650 ^{o}C for 5 h to obtain H-form.

The prepared carbon-templated ZSM-5 catalyst was denoted as C-ZSM5.

Phosphorous-modified C-ZSM5 catalysts were prepared by an impregnation method as shown in Fig. 2.3. Typical procedures for the preparation of phosphorous-modified C-ZSM5 catalysts are as follows. A known amount of phosphoric acid (H_3PO_4, Samchun Chem.) was dissolved in 10 ml of distillate water. 1 g of C-ZSM5 catalyst was then dispersed into the solution with constant stirring, and the mixture was stirred for 5 h at 40 ^{o}C. The resulting solid was dried overnight at 100 ^{o}C and calcined at 650 ^{o}C for 5 h. The phosphorous-modified C-ZSM5 catalysts were denoted as XP/C-ZSM5 (X=0.17, 0.3, 0.7, 1.4, and 2.7), where X represented wt% of phosphorous content.

Hydrothermal treatment of the prepared catalysts was performed in order to investigate the effect of phosphorous modification on the hydrothermal stability. The samples were charged into the fixed-bed reactor, and the temperature increased at a heating rate of 5 ^{o}C/min to 700 ^{o}C. The liquid water was then pumped into the preheated zone of the reactor at a flow rate of 0.2 g/min for 3 h. The hydrothermal treated catalysts were denoted as C-ZSM5-St., and *X*P/C-ZSM5-St. (*X*=0.17, 0.3, 0.7, 1.4, and 2.7), respectively.

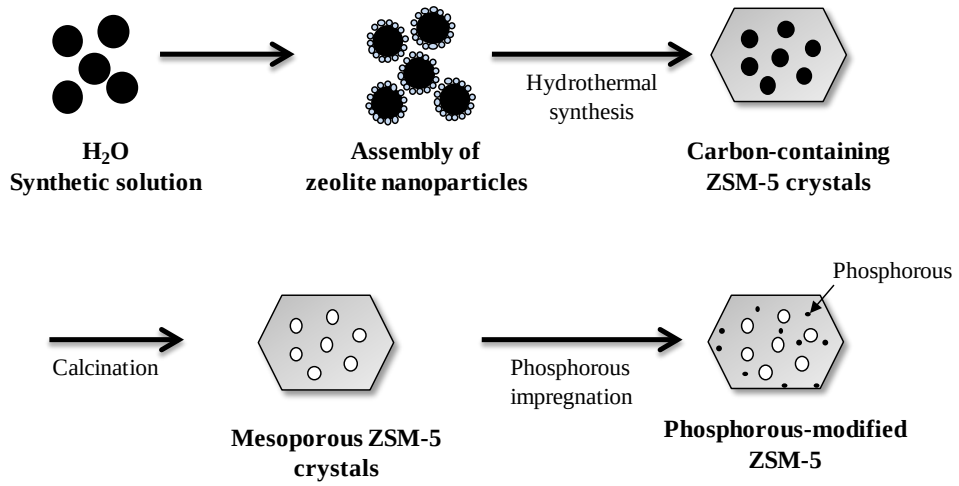

Fig. 2.3. Schematic procedures for the preparation of phosphorous modified micro/mesoporous ZSM-5 catalysts.

2.1.4. Lanthanum-containing phosphorous-modified porous ZSM-5 catalysts

A micro/mesoporous ZSM-5 catalyst was prepared by a carbon-templating method. Colloidal silica (Ludox HS-40, Sigma-Aldrich) and sodium aluminate ($NaAlO_2$, Junsei) were used as silicon and aluminum sources, respectively. Tetrapropylammonium bromide (TPABr, Sigma-Aldrich) and carbon (BP2000, Carbot Corp.) were used as a template and a secondary template, respectively, for the preparation of microporous and mesoporous ZSM-5 catalyst. Molar composition of $Si:Al:Na_2O:TPABr:H_2O$ was fixed at 1:0.03:0.07:0.03:35. An appropriate amount of sodium hydroxide (NaOH, Samchun Chem.) was dissolved in distilled water at 40 ^oC. Tetrapropylammonium bromide and colloidal silica were added into the sodium hydroxide solution under vigorous stirring, and the mixture was stirred until a homogeneous solution was obtained (Solution A). A known amount of sodium aluminate ($NaAlO_2$, Junsei) was separately dissolved in distilled water (Solution B). Solution B was then added into Solution A. After stirring the mixed solution at 40 ^oC for 3 h, carbon template was added under stirring for additional 3 h. The amount of carbon template was 30 wt% with respect to that of silicon source. The crystallization was carried out under static conditions in a Teflon-lined autoclave at 160 ^oC for 72 h. After crystallization, the resultant was filtered and washed with distilled water several times to obtain a solid product. The solid product was dried overnight at 110 ^oC, and it was finally calcined at 650 ^oC for 10 h in an air stream to

remove carbon and organic templates. The catalyst was ion-exchanged three times with 1 M solution of ammonium nitrate (NH_4NO_3, Junsei) at 80 ^oC for 3 h. The ion-exchanged catalyst was finally calcined at 650 ^oC for 5 h to obtain H-form. The prepared carbon-templated ZSM-5 catalyst was denoted as C-ZSM5.

Phosphorous-modified C-ZSM5 catalyst was prepared by an impregnation method. The phosphorous loading was fixed at 0.3 wt%. An appropriate amount of phosphoric acid (H_3PO_4, Samchun Chem.) was dissolved in 10 ml of distillate water. 1 g of C-ZSM5 catalyst was then dispersed into the solution under vigorous stirring, and the mixture was stirred at 40 ^oC for 5 h. The resulting solid was dried overnight at 100 ^oC and calcined at 650 ^oC for 5 h. The phosphorous-modified C-ZSM5 catalyst was denoted as P/C-ZSM5.

Lanthanum was introduced into P/C-ZSM5 catalyst by an impregnation method as shown in Fig. 2.4. A known amount of lanthanum nitrate ($La(NO_3)_3 \cdot 6H_2O$, Sigma-Aldrich) was dissolved in 10 ml of distillate water. 1 g of P/C-ZSM5 catalyst was then added into the solution with constant stirring. After stirring the mixture at 40 ^oC for 3 h, the solid product was dried overnight at 100 ^oC, and then it was calcined at 650 ^oC for 5 h to yield a lanthanum-containing P/C-ZSM5 catalyst. The lanthanum-containing P/C-ZSM5 catalysts were denoted as LaX-P/C-ZSM5 (X=0.3, 0.7, 0.9, and 1.2), where X represented La/Al ratio in the catalyst.

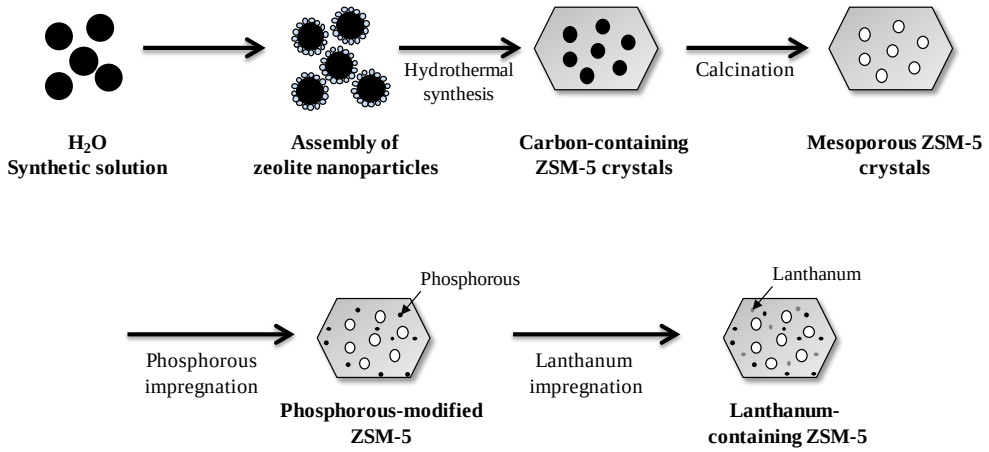

Fig. 2.4. Schematic procedures for the preparation of lanthanum-containing phosphorous modified micro/mesoporous ZSM-5 catalysts.

2.2. Characterization

2.2.1. Physicochemical property of catalysts

Chemical composition of the catalyst was measured by inductively coupled plasma-atomic emission spectrometry (ICP-AES) analysis (Shimadzu, ICPS-7500). Crystalline phases of the catalysts were investigated by XRD measurements (Rigaku, D-MAX2500-PC) using Cu-Kα radiation (λ=1.54056 Å) operated at 50 kV and 100 mA. Surface areas of the catalysts were calculated using the BET equation, and pore volumes were determined by the BJH (Barret-Joyner-Hallender) method applied to the desorption branch of the isotherms. FT-IR (Fourier transform infrared) spectra were obtained using an infrared spectrophotometer (ThermoFisher Scientific, Nicolet 6700) equipped with a diffuse reflectance accessory. Chemical states of aluminum species in the catalysts were examined by ^{27}Al MAS NMR analysis (Bruker, AVANCE II) at a MAS frequency of 11 kHz. The amount of carbon deposition in the used catalysts was determined by CHNS elemental analysis (CHNS 932, Leco). High resolution-transmission electron microscopy (HR-TEM) analyses (Jeol, JEM-3000F) were conducted to see the morphologies of the catalysts.

2.2.2. Acid property of catalysts

NH_3-TPD (temperature-programmed desorption) experiments were performed to determine the acid property of the catalysts (BEL Japan, BELCAT-B). 0.07 g of each catalyst charged into the TPD apparatus was pretreated at 200 ^oC for 2 h with a stream of helium (50 ml/min). After cooling the catalyst to room temperature, ammonia (50 ml/min) was introduced into the reactor at 50 ^oC for 30 min to saturate acid sites of the catalyst. Physisorbed ammonia was removed at 100 ^oC for 1 h under a flow of helium (50 ml/min). After cooling down the sample, furnace temperature was increased from 50 ^oC to 650 ^oC at a heating rate of 5 ^oC/min under a flow of helium (30 ml/min). The desorbed ammonia was detected using a TCD (thermal conductivity detector).

2.2.3. Base property of catalysts

CO_2-TPD experiments were carried out in order to measure the basicity of the catalysts. 0.1g of each catalyst charged into the TPD apparatus was pretreated at 200 ^oC for 1 h with a stream of helium (20 ml/min). After cooling the catalyst to room temperature, 20 ml of CO_2 was pulsed into the reactor every minute under a flow of helium (5 ml/min) until base sites of the catalyst were saturated with CO_2. Physisorbed CO_2 was removed by evacuating the catalyst sample at 100 ^oC for 1 h. After cooling down the sample, furnace temperature was increased from 50 ^oC to 700 ^oC at a heating rate of 5 ^oC/min under a flow of helium (10 ml/min). The desorbed CO_2 was detected using a GC-MSD (Agilent, MSD-6890 N GC).

2.2.4. Adsorption ability of catalyst for n-pentane

n-Pentane TPD experiments were conducted to determine the adsorption ability of the catalysts. Each catalyst (0.08 g) was charged into a conventional TPD apparatus. The catalyst was pretreated at 200 ^{o}C for 2 h under a flow of helium (40 ml/min) to remove any physisorbed organic molecules. n-Pentane (0.83 μl/min) was then introduced into the reactor at 100 ^{o}C for 30 min under a flow of helium (40 ml/min) in order to saturate the adsorption sites of the catalyst. The physisorbed n-pentane was removed by evacuating the sample at 50 ^{o}C for 30 min. After cooling down the sample, furnace temperature was increased from room temperature to 600 ^{o}C at a heating rate of 5 ^{o}C/min under a flow of helium (30 ml/min). The desorbed molecules were detected using a GC-MSD (Agilent, MSD-6890 N GC).

2.3. Catalytic cracking of C_5 raffinate

Catalytic cracking of C_5 raffinate was carried out in a continuous flow fixed-bed reactor under atmospheric pressure. The composition of C_5 raffinate is listed in Table 2.2. Prior to the catalytic reaction, each catalyst (150 mg) was pretreated at 600 ^oC for 1 h with a nitrogen stream (40 ml/min). C_5 raffinate was then sufficiently vaporized by passing through a preheating zone, and it was continuously fed into the reactor together with nitrogen carrier (40 ml/min), as shown in Fig. 2.5. The catalytic reaction was carried out at 500-600 ^oC. WHSV (weight hourly space velocity) was fixed at 3.5 h^{-1}. Reaction products were periodically sampled and analyzed using an on-line gas chromatograph (Younglin ACME 6100) equipped with a FID (flame ionization detector). Conversion of C_5 raffinate and selectivity for light olefins (ethylene and propylene) were calculated on the basis of carbon balance as follows. Yield for light olefins (ethylene and propylene) was calculated by multiplying conversion of C_5 raffinate and selectivity for light olefins (ethylene and propylene).

Conversion of C_5 raffinate

$$= \frac{\text{moles of } C_5 \text{ raffinate reacted}}{\text{moles of } C_5 \text{ raffinate supplied}} \times 100 \qquad (2.1)$$

Selectivity for light olefins (ethylene and propylene)

$$= \frac{\text{moles of ethylene and propylene formed}}{\text{moles of } C_5 \text{ raffinate reacted}} \times 100 \qquad (2.2)$$

Table 2.2

Composition of C_5 raffinate

Component	wt%
Pentane	33.4
2-Methyl-butane	25.0
1-Pentene	8.3
2-Methyl-2-butene	25.0
Cyclopentane	8.3

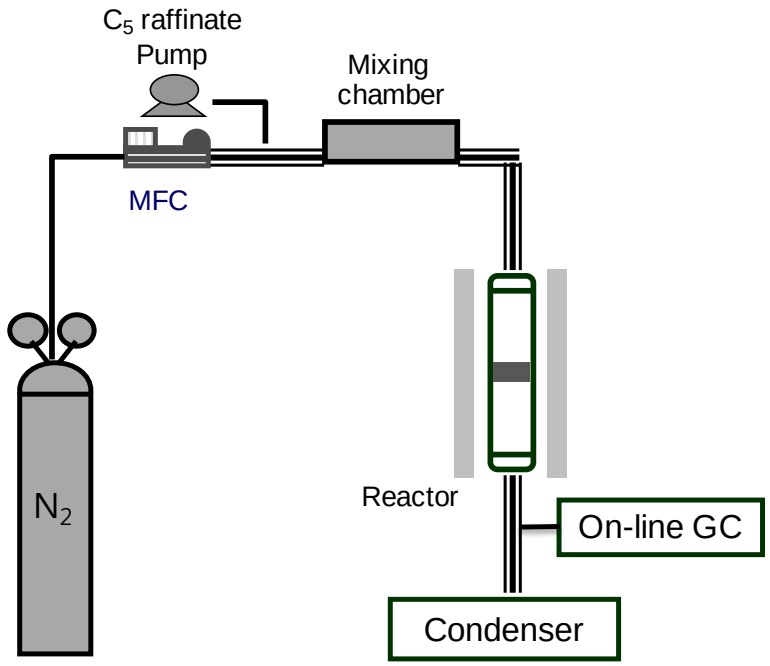

Fig. 2.5. Scheme of reaction system for catalytic cracking of C_5 raffinate to light olefins.

Chapter 3. Results and Discussion

3.1. Characterization and catalytic activity of micro/mesoporous ZSM-5 catalysts prepared by soft templating method

3.1.1. Characterization of PAM(X)-ZSM5 (X=0, 0.12, 0.25, 0.53, 0.64, and 0.78) catalysts

Textural properties of PAM(X)-ZSM5 (X=0, 0.12, 0.25, 0.53, 0.64, and 0.78) catalysts were examined by nitrogen adsorption-desorption isotherm measurements. Fig. 3.1 shows the nitrogen adsorption-desorption isotherms of PAM(X)-ZSM5 catalysts. PAM(0)-ZSM5 catalyst exhibited type-I isotherm, a typical feature of microporous materials. On the other hand, PAM(X)-ZSM5 (X=0.12, 0.25, 0.53, 0.64, and 0.78) catalysts exhibited type-IV isotherm with a hysteresis loop at 0.45-0.95, indicating the existence of mesopores in the catalysts. The amount of volume adsorbed on the catalyst increased with increasing PAM content. Detailed textural properties of PAM(X)-ZSM5 (X=0, 0.12, 0.25, 0.53, 0.64, and 0.78) catalysts are summarized in Table 3.1. BET surface area and micropore volume of PAM(X)-ZSM5 (X=0.12, 0.25, 0.53, 0.64, and 0.78) catalysts were slightly lower than those of PAM(0)-ZSM5 catalyst. This is because PAM partly affected the crystallization of ZSM5. Less crystallized ZSM5 has defect sites on the ZSM5 crystal, leading to lower

surface area and lower micropore volume [62]. On the other hand, mesopore volume of the catalysts increased with increasing PAM content. Thus, mesoporous ZSM5 catalysts could be successfully synthesized using a PAM-templating method and mesoporosity of the catalysts could be controlled by adjusting PAM content.

FE-SEM and HR-TEM analyses were conducted to see the morphologies of the catalysts. Fig. 3.2 (a) and 3.2 (b) show the FE-SEM images of PAM(0)-ZSM5 and PAM(0.25)-ZSM5 catalysts. Although both PAM(0)-ZSM5 and PAM(0.25)-ZSM5 catalysts exhibited well-developed and highly crystallized images, their surface morphologies were quite different. Compared to microporous PAM(0)-ZSM5 catalyst, mesoporus PAM(0.25)-ZSM5 catalyst showed rough surface morphology due to the formation of mesopores. Fig. 3.2 (c) and Fig. 3.2 (d) show the HR-TEM images of PAM(0)-ZSM5 and PAM(0.25)-ZSM5 catalysts. HR-TEM image of PAM(0)-ZSM5 showed straight 10-ring microporous channels throughout the entire particle. However, PAM(0.25)-ZSM5 catalyst exhibited thin slices perpendicular to the microporous channels, which were assigned to mesopores generated by the removal of organic template after calcination.

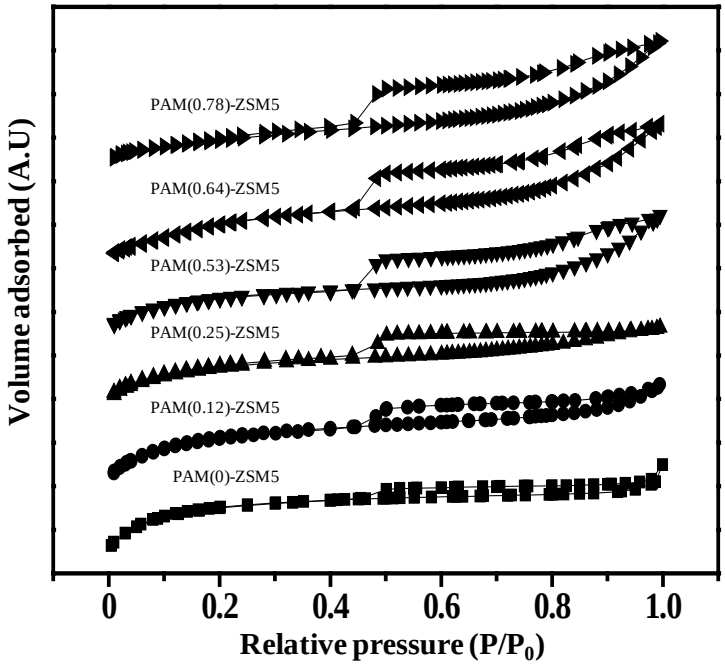

Fig. 3.1. Nitrogen adsorption-desorption isotherms of PAM(X)-ZSM5 (X=0, 0.12, 0.25, 0.53, 0.64, and 0.78) catalysts.

Table 3.1

Chemical and physical properties of PAM(X)-ZSM5 (X=0, 0.12, 0.25, 0.53, 0.64, and 0.78) catalysts

Catalyst	Surface area (m^2/g) [a]	Pore volume (cm^3/g) [b]	
		Micropore	Mesopore
PAM(0)-ZSM5	375.5	0.147	-
PAM(0.12)-ZSM5	351.6	0.134	0.049
PAM(0.25)-ZSM5	334.7	0.131	0.071
PAM(0.53)-ZSM5	317.5	0.119	0.092
PAM(0.64)-ZSM5	313.2	0.114	0.106
PAM(0.78)-ZSM5	311.9	0.102	0.109

[a] Calculated by BET (Brunauer-Emmett-Teller) equation
[b] BJH (Barret-Joyner-Hallender) desorption pore volume

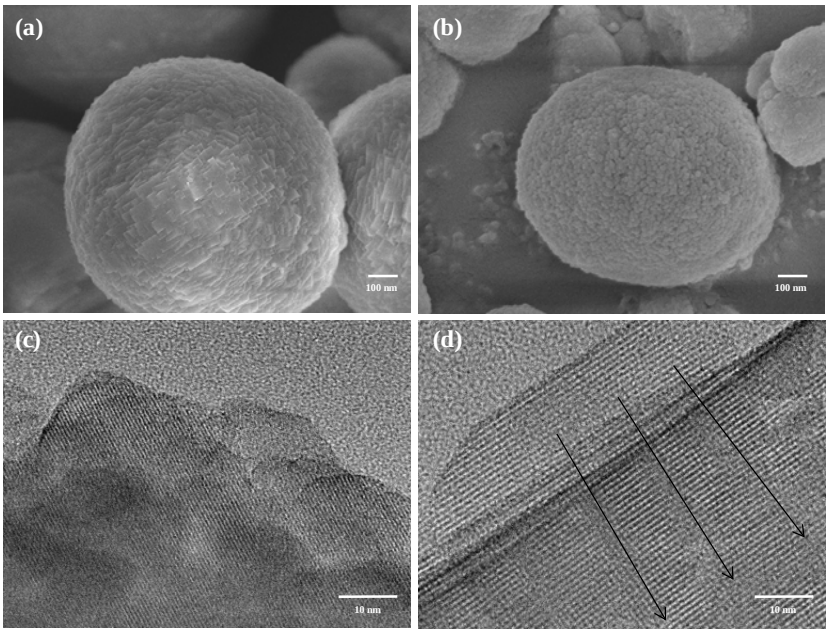

Fig. 3.2. FE-SEM images of (a) PAM(0)-ZSM5 and (b) PAM(0.25)-ZSM5, and HR-TEM images of (c) PAM(0)-ZSM5 and (d) PAM(0.25)-ZSM5.

3.1.2. Crystalline Structure of PAM(X)-ZSM5 (X=0, 0.12, 0.25, 0.53, 0.64, and 0.78) catalysts

Fig. 3.3 shows the XRD patterns of PAM(X)-ZSM5 (X=0, 0.12, 0.25, 0.53, 0.64, and 0.78) catalysts. All the catalysts showed the characteristic peaks associated with ZSM5, and no additional phases were observed [63]. However, PAM(0.78)-ZSM5 catalyst exhibited weak peak intensity compared to the other catalysts, indicating that crystallinity of PAM(0.78)-ZSM5 catalyst significantly decreased. It has been reported that zeolite nucleation takes place on the surface between polymer networks and zeolite synthesis gel when water-soluble polymer is added into the synthesis gel [64]. As zeolite crystal grows, the incorporated polymer becomes separated from the zeolite matrix, and finally, intracrystal mesopores are formed after calcination by the removal of organic polymer. However, crystallinity of ZSM5 decreases when an excess amount of soft template is introduced into the synthesis gel, because large amount of soft template prohibits the incorporation of Si and Al around the structure directing agent of ZSM5 (TPABr).

Fig. 3.4 shows the FT-IR spectra of PAM(0)-ZSM5, PAM(0.25)-ZSM5, PAM(0.64)-ZSM5, and PAM(0.78)-ZSM5 catalysts. The characteristic IR bands of the catalysts appeared at 450, 550, 795 and 1224 cm^{-1}. The bands at 450 cm^{-1} (T-O band), 795 cm^{-1} (external symmetric stretch), and 1224 cm^{-1} (external asymmetric stretch) are typical bands for highly siliceous materials [65]. On the other hand, the band at 550 cm^{-1} is attributed to the five-ring units presented in ZSM5, and therefore, it can be used to determine the crystallinity

of ZSM5 [66]. Compared to PAM(X)-ZSM5 (X=0, 0.25, and 0.64) catalysts, PAM(0.78)-ZSM5 catalyst showed weak band intensity at 550 cm^{-1}. This result indicates that the addition of excess amount of PAM template into synthesis gel caused low crystallinity of PAM(0.75)-ZSM5 catalyst, in good agreement with the XRD results (Fig. 3.3).

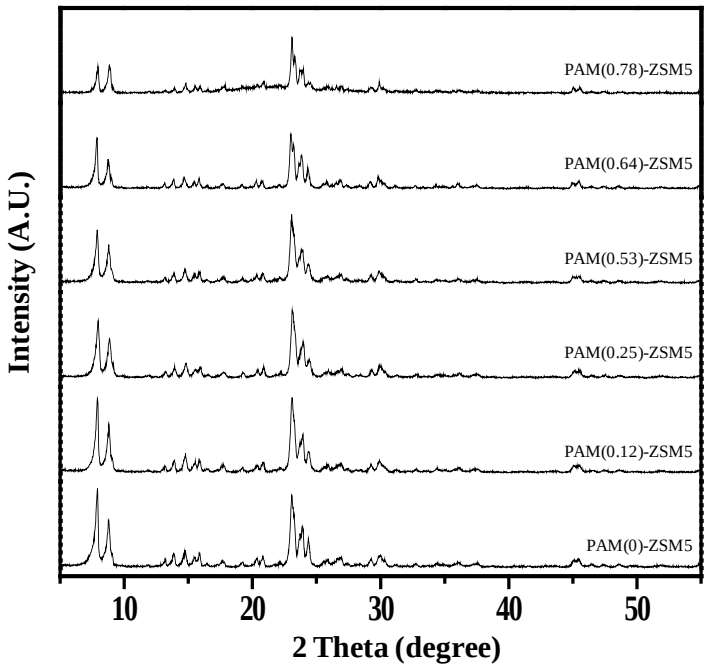

Fig. 3.3. XRD patterns of PAM(X)-ZSM5 (X=0, 0.12, 0.25, 0.53, 0.64, and 0.78) catalysts.

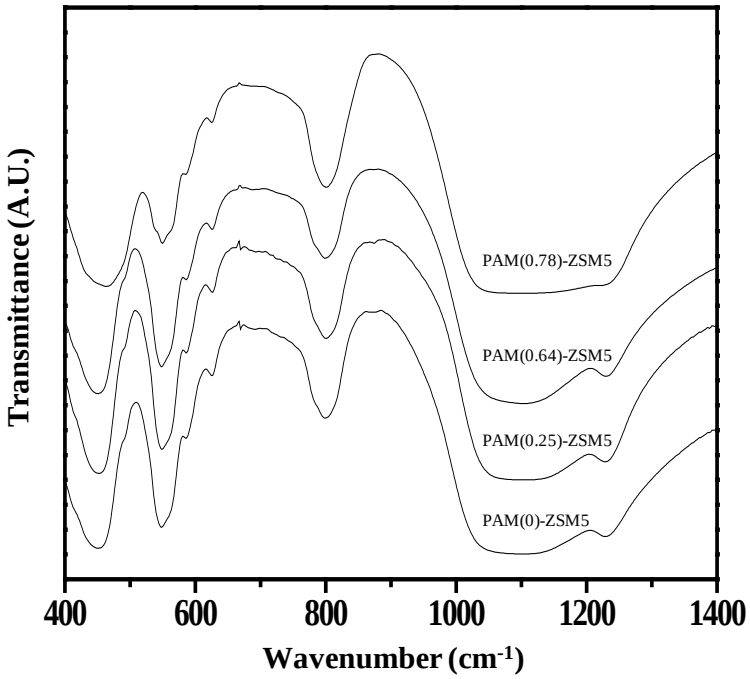

Fig. 3.4. FT-IR spectra of PAM(0)-ZSM5, PAM(0.25)-ZSM5, PAM(0.64)-ZSM5, and PAM(0.78)-ZSM5 catalysts.

3.1.3. Acid property of PAM(X)-ZSM5 (X=0, 0.12, 0.25, 0.53, 0.64, and 0.78) catalysts

In the catalytic cracking reaction, acid property of the catalysts is an important factor determining the catalytic performance [67]. Therefore, NH_3-TPD experiments were conducted to investigate the acid property of PAM(X)-ZSM5 (X=0, 0.12, 0.25, 0.53, 0.64, and 0.78) catalysts. Fig. 3.5 shows the NH_3-TPD profiles of PAM(X)-ZSM5 catalysts. All the catalysts showed two major desorption peaks at around 150 ^{o}C and 360 ^{o}C corresponding to weak acid site and strong acid site, respectively. Acidity of PAM(X)-ZSM5 catalysts determined from TPD peak area is summarized in Table 3.2. It was revealed that acidity of PAM(0.78)-ZSM5 catalyst was significantly lower than that of PAM(X)-ZSM5 (X=0, 0.12, 0.25, 0.53, and 0.64) catalysts. This is because incorporation of Al and Si was suppressed under excess amount of PAM content, leading to the decreased acidity of PAM(0.78)-ZSM5 catalyst.

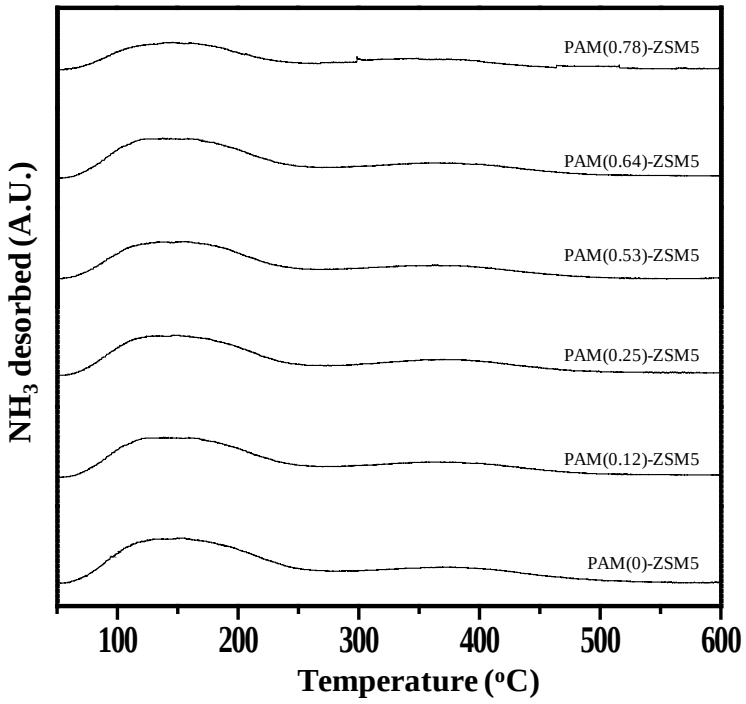

Fig. 3.5. NH_3-TPD profiles of PAM(X)-ZSM5 (X=0, 0.12, 0.25, 0.53, 0.64, and 0.78) catalysts.

Table 3.2

Acidity of PAM(X)-ZSM5 (X=0, 0.12, 0.25, 0.53, 0.64, and 0.78) catalysts.

Catalyst	Acidity (mmol-NH_3/g)
PAM(0)-ZSM5	129.2
PAM(0.12)-ZSM5	126.9
PAM(0.25)-ZSM5	123.5
PAM(0.53)-ZSM5	119.6
PAM(0.64)-ZSM5	119.2
PAM(0.78)-ZSM5	79.4

3.1.4. Adsorption ability of PAM(X)-ZSM5 (X=0, 0.12, 0.25, 0.53, 0.64, and 0.78) catalysts

Adsorption ability of PAM(X)-ZSM5 (X=0, 0.12, 0.25, 0.53, 0.64, and 0.78) catalysts for n-pentane was measured by n-pentane TPD experiments. Fig. 3.6 shows the n-pentane TPD profiles of PAM(X)-ZSM5 catalysts. All the catalysts exhibited a desorption peak at around 140 ^{o}C. Undoubtedly, the area of TPD profile reflects the amount of n-pentane adsorbed on the catalyst. As shown in Fig. 3.6, the area of TPD profile of the catalysts increased with increasing PAM content. This result indicates that adsorption ability of PAM(X)-ZSM5 catalysts increased with increasing mesopore volume of the catalysts (Table 3.1). It has been reported that mesoporous zeolite not only accelerates the diffusion rate but also increases the adsorption capacity for certain molecules in comparison with microporous zeolite [68]. From the n-pentane TPD results, it can be inferred that n-pentane was more readily diffused into mesoporous ZSM5 than into microporous ZSM5.

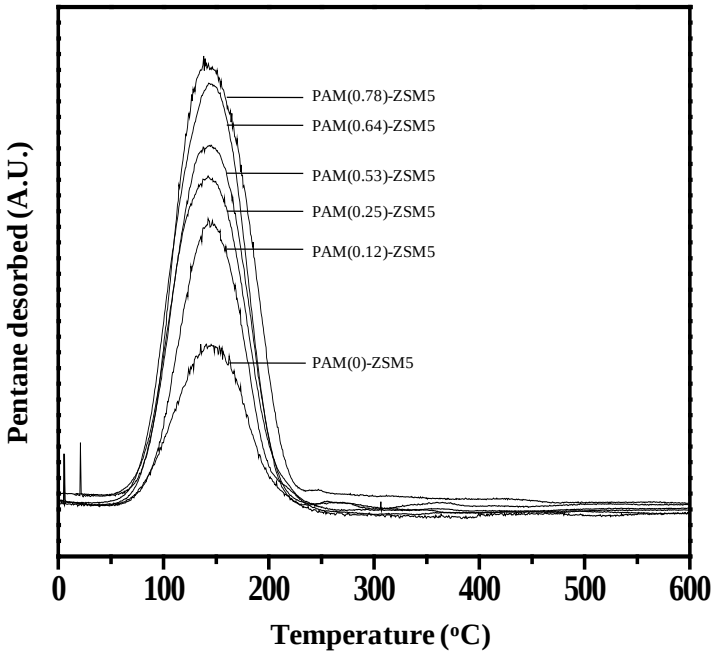

Fig. 3.6. n-Pentane TPD profiles of PAM(X)-ZSM5 (X=0, 0.12, 0.25, 0.53, 0.64, and 0.78) catalysts.

3.1.5. Effect of mesoporosity of PAM(X)-ZSM5 (X=0, 0.12, 0.25, 0.53, 0.64, and 0.78) catalysts on the catalytic performance

Correlations between mesopore/micropore volume ratio and catalytic cracking activity have been made to investigate the effect of mesoporsity on the catalytic performance. Fig. 3.7 shows the correlations between mesopore/micropore volume ratio and catalytic performance of PAM(X)-ZSM5 catalysts in the catalytic cracking of C_5 raffinate to light olefins (ethylene and propylene). The correlations clearly show that catalytic performance of PAM(X)-ZSM5 catalysts was closely related to the mesoporosity of the catalysts. Conversion of C_5 raffinate and yield for light olefins showed volcano-shaped trends with respect to mesopore/micropore volume ratio of the catalysts. The improved catalytic performance of PAM(X)-ZSM5 (X=0.12, 0.25, 0.53, and 0.64) catalysts was attributed to the formation of mesopores inside ZSM5 crystals, which enhanced the accessibility of reactants and reaction intermediates into the active sites of the catalysts. As discussed in the NH_3-TPD results, however, PAM(0.78)-ZSM5 catalyst retained much smaller acidity than PAM(X)-ZSM5 (X=0.12, 0.25, 0.53, and 0.64) catalysts. Therefore, PAM(0.78)-ZSM5 catalyst with small acidity exhibited a lower catalytic activity than PAM(X)-ZSM5 (X=0.12, 0.25, 0.53, and 0.64) catalysts, although PAM(0.78)-ZSM5 catalyst had the highest mesopore volume. Thus, an optimal PAM content was required for maximum production of light olefins through catalytic cracking of C_5 raffinate. Among the catalysts tested, PAM(0.64)-ZSM5 catalyst showed the best catalytic

performance in terms of conversion of C_5 raffinate and yield for light olefins.

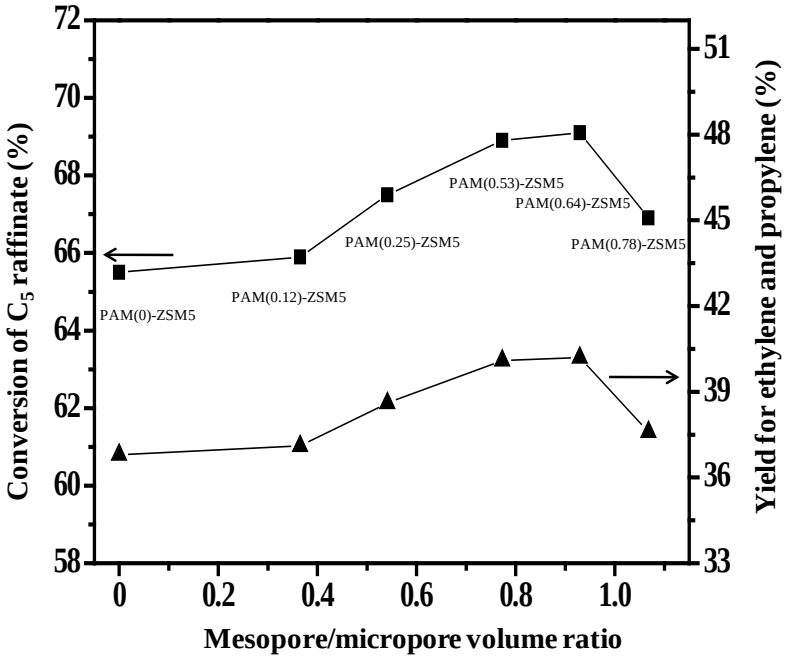

Fig. 3.7. Correlations between mesopore/micropore volume ratio and catalytic performance of PAM(X)-ZSM5 (X=0, 0.12, 0.25, 0.53, 0.64, and 0.78) catalysts.

3.2. Characterization and catalytic activity of micro/mesoporous ZSM-5 catalysts prepared by hard templating method

3.2.1. Characterization of C(X)-ZSM-5 (X=0, 10, 20, 30, 40, and 50) catalysts

Successful formation of carbon-templated ZSM-5 catalysts was examined by XRD measurement. Fig. 3.8 XRD patterns of C(X)-ZSM-5 (X=0, 10, 20, 30, 40, and 50) catalysts. All the catalysts showed the typical intrinsic crystalline structure of ZSM-5, and no additional phase was observed [63]. This indicates that C(X)-ZSM-5 catalysts were successfully prepared even though carbon was used as a secondary template. However, C(40)-ZSM-5 and C(50)-ZSM-5 catalysts exhibited slightly weak peak intensity compared to the other catalysts. This might be due to the fact that large amount of carbon template affected the formation of high crystallinity of ZSM-5. The catalyst produced with large amount of carbon template (> 40 wt%) generated many vacant sites by forming mesopores, leading to low crystallinity.

Si/Al atomic ratios of C(X)-ZSM-5 (X=0, 10, 20, 30, 40, and 50) catalysts determined by ICP-AES analyses are listed in Table 3.3. Si/Al atomic ratios of carbon-templated ZSM-5(C(X)-ZSM-5 (X=10, 20, 30, 40, and 50) catalysts and pure ZSM-5 (C(0)-ZSM-5) catalyst were nearly identical, and these values were in good agreement with the designed value

(Si/Al=30). This means that silicon precursor and aluminum precursor successfully interacted without significant loss, and carbon did not disrupt the formation of aluminosilicate.

Textural properties of C(X)-ZSM-5 (X=0, 10, 20, 30, 40, and 50) catalysts were examined by nitrogen adsorption-desorption isotherm measurements. Fig. 3.9 (a) shows the nitrogen adsorption-desorption isotherms of C(X)-ZSM-5 catalysts. It was found that C(0)-ZSM-5 catalyst exhibited type-I isotherm, typical characteristics of microporous materials. After carbon was used as a secondary template, however, isotherms were transformed from type-I isotherm to type-IV isotherm with obvious hysteresis loop at relative pressure higher than 0.4, indicating the existence of mesopores. It was also found that hysteresis loop of C(X)-ZSM-5 catalysts was changed from H4 type to H3 type with increasing carbon content, indicating the generation of slit-like pores with increasing carbon content [57]. The amount of volume adsorbed on the catalyst increased with increasing carbon template content. Fig. 3.9 (b) shows the BJH pore size distributions of C(X)-ZSM-5 catalysts obtained from desorption branches. C(0)-ZSM-5 catalyst showed the micropore size distribution, while C(X)-ZSM-5 (X=10, 20, 30, 40, and 50) catalysts showed both micropore and mesopore size distributions. This result also supports that mesopores were generated in the ZSM-5 catalyst when carbon was used as a secondary template. C(X)-ZSM-5 (X=10, 20, 30, 40, and 50) catalysts exhibited a narrow mesopore size distribution centered at around 3.5-4.5 nm. In addition, mesopores were well developed with increasing carbon template content.

Detailed textural properties of C(X)-ZSM-5 (X=0, 10, 20, 30, 40, and

50) catalysts are summarized in Table 3.3. BET surface area and micropore volume of the catalysts showed no great difference with respect to carbon template content, indicating that surface area and micropore volume were not affected by carbon template content. However, mesopore volume of the catalysts was strongly influenced by carbon template content. Mesopore volume of the catalysts increased with increasing carbon template content. This implies that carbon template content in the C(X)-ZSM-5 catalysts served as an important factor determining the mesoporous textural properties of the catalysts.

HR-TEM analyses were conducted in order to confirm the formation of mesopores in the C(X)-ZSM-5 catalysts. Fig. 3.10 shows the HR-TEM images of C(0)-ZSM-5, C(30)-ZSM-5, and C(50)-ZSM-5 catalysts calcined at 550 ^{o}C. HR-TEM results revealed that surface morphologies of the catalyst were strongly affected by carbon template content. C(30)-ZSM-5 and C(50)-ZSM-5 catalysts showed bright parts on the crystal, indicative of existence of mesopores. On the other hand, C(0)-ZSM-5 catalyst showed no mesoporous nature. C(30)-ZSM-5 and C(50)-ZSM-5 catalysts exhibited less dense crystal image than C(0)-ZSM-5 catalyst, which was attributed to the vacant sites resulting from removal of carbon particles. It was also observed that C(50)-ZSM-5 catalyst exhibited a more randomly distributed pore structure than C(30)-ZSM-5 catalyst. This might be due to partial aggregation of carbon particles when an excess amount of carbon was used in the preparation of C(X)-ZSM-5 catalysts.

It has been reported that mesoporous zeolites can be classified into three different types depending on the preparation method; hierarchical zeolite

crystals, nanosized zeolite crystals, and supported zeolite crystals [68]. As shown in Fig. 3.10, C(0)-ZSM-5 catalyst exhibited a typical form of ZSM-5. On the other hand, C(30)-ZSM-5 and C(50)-ZSM-5 catalysts showed a hierarchical ZSM-5 crystal form with additional pores. Carbon material was encapsulated in the ZSM-5 crystal during the hydrothermal synthesis, and it was burned out during the calcination step, resulting in the formation of intracrystalline mesopores in the single crystal. All the prepared catalysts had uniform crystal size of 0.8-1.2 μm.

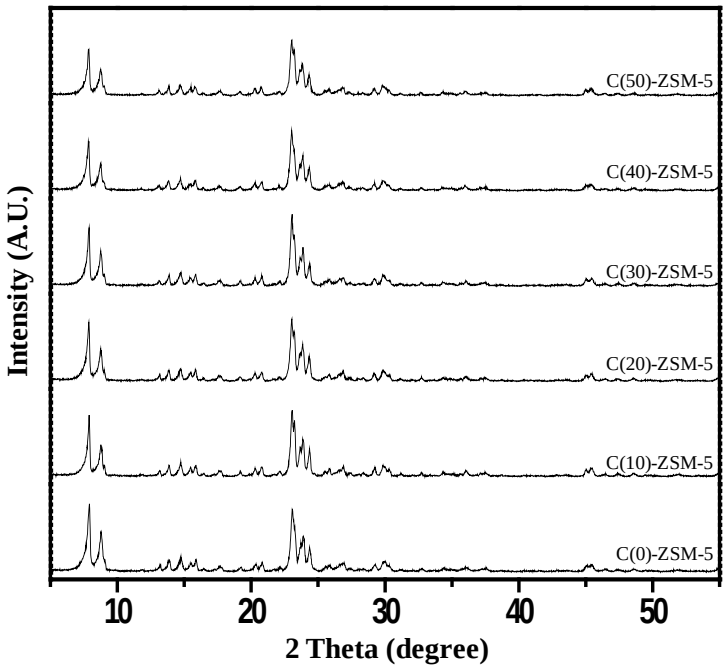

Fig. 3.8. XRD patterns of C(X)-ZSM-5 (X=0, 10, 20, 30, 40, and 50) catalysts.

Table 3.3

Chemical and physical properties of C(X)-ZSM-5 (X=0, 10, 20, 30, 40, and 50) catalysts

Catalyst	Si/Al atomic ratio [a]	Surface area (m^2/g) [b]	Pore volume (cm^3/g) [c]	
			Micropore	Mesopore
C(0)-ZSM-5	29.2	391.5	0.155	-
C(10)-ZSM-5	28.7	385.5	0.145	0.068
C(20)-ZSM-5	29.5	390.5	0.147	0.086
C(30)-ZSM-5	28.9	396.4	0.146	0.131
C(40)-ZSM-5	28.6	390.5	0.143	0.223
C(50)-ZSM-5	28.7	372.7	0.142	0.286

[a] Determined by ICP-AES measurement
[b] Calculated by BET (Brunauer-Emmett-Teller) equation
[c] BJH (Barret-Joyner-Hallender) desorption pore volume

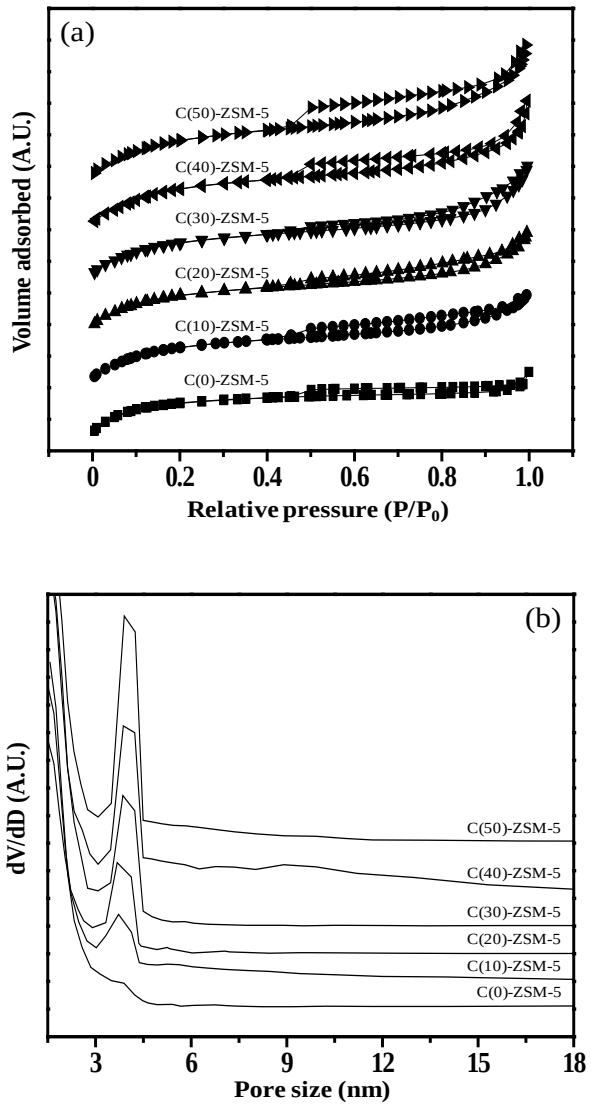

Fig. 3.9. (a) Nitrogen adsorption-desorption isotherms and (b) pore size distributions of C(X)-ZSM-5 (X=0, 10, 20, 30, 40, and 50) catalysts.

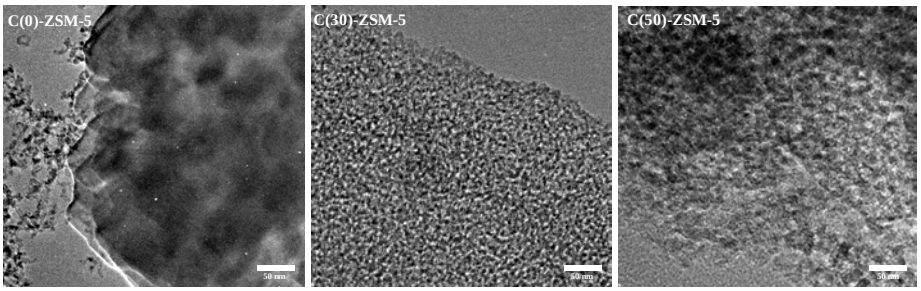

Fig. 3.10. HR-TEM images of C(0)-ZSM-5, C(30)-ZSM-5, and C(50)-ZSM-5 catalysts.

3.2.2. Acid property of C(X)-ZSM-5 (X=0, 10, 20, 30, 40, and 50) catalysts

NH_3-TPD experiments were conducted with an aim of determining the acid property of C(X)-ZSM-5 (X=0, 10, 20, 30, 40, and 50) catalysts. Fig. 3.11 shows the NH_3-TPD profiles of C(X)-ZSM-5. All the catalysts showed two major desorption peaks at around 130 ^oC and 430 ^oC. Acidity of the C(X)-ZSM-5 catalysts determined from TPD peak area is summarized in Table 3.4. Acidity of C(X)-ZSM-5 (X=10, 20, 30, 40, and 50) catalysts was almost identical to that of C(0)-ZSM-5 catalyst. This result indicates that acid property of C(X)-ZSM-5 catalysts was not influenced by carbon template content.

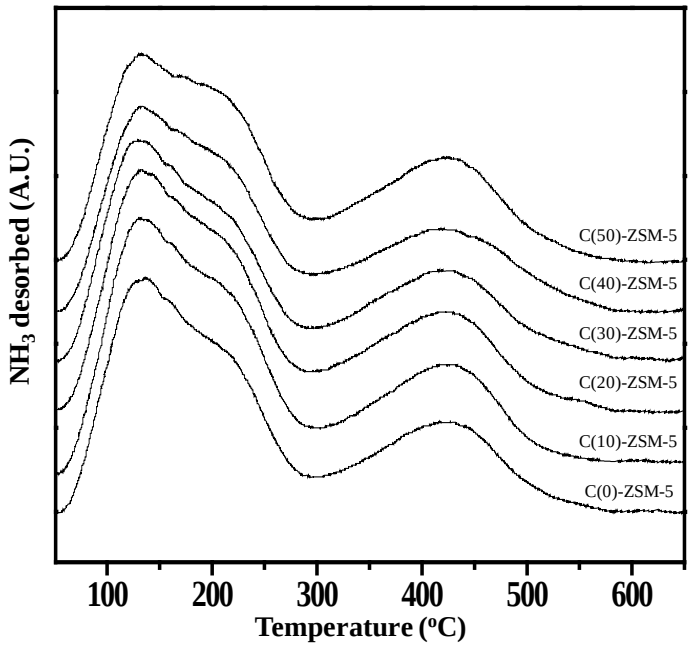

Fig. 3.11. NH_3-TPD profiles of C(X)-ZSM-5 (X=0, 10, 20, 30, 40, and 50) catalysts.

Table 3.4

Acidity of C(X)-ZSM-5 (X=0, 10, 20, 30, 40, and 50) catalysts

Catalyst	Acidity (mmol-NH_3/g)
C(0)-ZSM-5	0.141
C(10)-ZSM-5	0.139
C(20)-ZSM-5	0.138
C(30)-ZSM-5	0.140
C(40)-ZSM-5	0.135
C(50)-ZSM-5	0.133

3.2.3. Adsorption ability C(X)-ZSM-5 (X=0, 10, 20, 30, 40, and 50) catalysts

It has been reported that mesoporous zeolite not only accelerates the diffusion rate but also increases the adsorption capacity for certain molecules in comparison with microporous zeolite [56,69,70]. In order to examine the adsorption ability of C(X)-ZSM-5 (X=0, 10, 20, 30, 40, and 50) catalysts, n-pentane TPD experiments were conducted. Fig. 3.12 shows the n-pentane TPD profiles of C(X)-ZSM-5 (X=0, 10, 20, 30, 40, and 50) catalysts. All the catalysts exhibited a single peak at around 150 ^{o}C, which was attributed to desorption of n-pentane. Furthermore, no other molecules were detected. These results were in good agreement with the previous works [71,72]. It has been reported that n-hexane TPD over HZSM-5 (Si/Al ratio = 25) exhibited a single peak attributed to desorption of n-hexane [71]. n-Pentane TPD over silicalite also showed a single desorption peak due to desorption of n-pentane [72]. As reported in the previous studies [71,72], n-pentane was fully desorbed at temperature below 200 ^{o}C in this work. This temperature was not sufficient to crack n-pentane. Undoubtedly, the area of TPD profile reflects the amount of n-pentane adsorbed on the catalyst. As shown in Fig. 3.12, area of TPD profile for C(X)-ZSM-5 catalysts increased with increasing carbon template content. This result indicates that adsorption ability of C(X)-ZSM-5 catalysts increased with increasing mesopore volume of the catalyst (Table 3.3). From the n-pentane TPD result, it can be inferred that n-pentane was more readily diffused into mesoporous ZSM-5 than into microporous ZSM-5. Among the

catalysts examined, C(50)-ZSM-5 catalysts exhibited the highest adsorption ability for n-pentane.

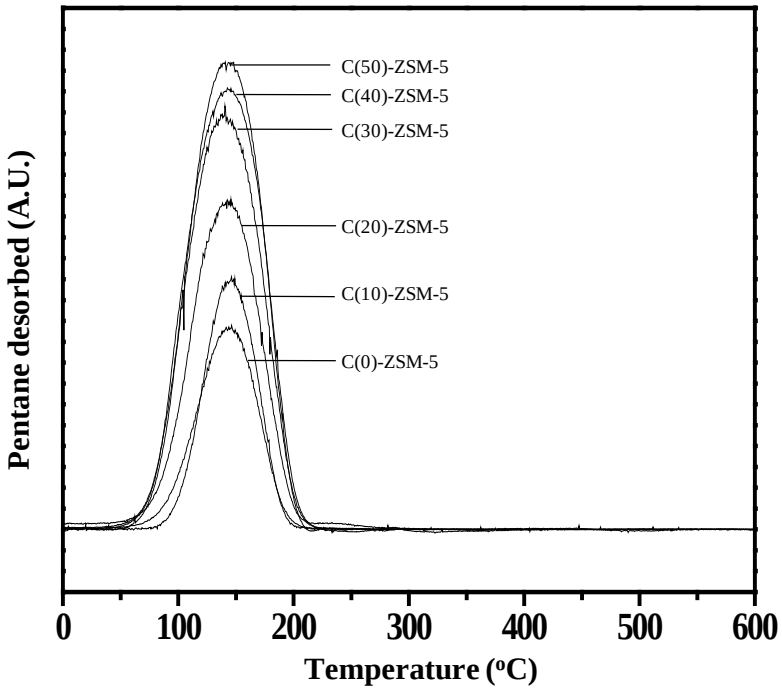

Fig. 3.12. n-Pentane TPD profiles of C(X)-ZSM-5 (X=0, 10, 20, 30, 40, and 50) catalysts.

3.2.4. Catalytic activity of C(X)-ZSM-5 (X=0, 10, 20, 30, 40, and 50) catalysts

Fig. 3.13 shows the catalytic performance of C(X)-ZSM-5 (X=0, 10, 20, 30, 40, and 50) catalysts in the catalytic cracking of C_5 raffinate to light olefins (ethylene and propylene) performed at 500 ^{o}C after a 3 h-catalytic reaction, plotted as a function of carbon template content. All the catalysts exhibited a stable catalytic performance during 3 h-catalytic reaction without a significant deactivation. Conversion of C_5 raffinate increased with increasing carbon template content, while selectivity for ethylene and propylene over the catalysts showed constant values. As a consequence, yield for light olefins increased with increasing carbon template content. Among the catalysts tested, C(50)-ZSM-5 catalyst showed the best catalytic performance in terms of conversion of C_5 raffinate and yield for light olefins.

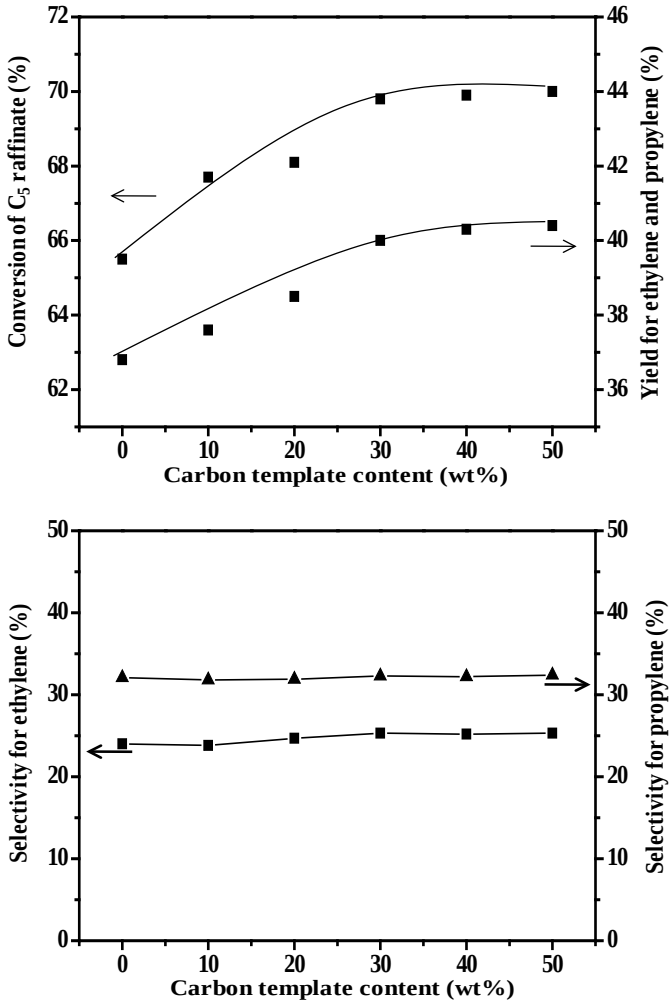

Fig. 3.13. Catalytic performance of C(X)-ZSM-5 (X=0, 10, 20, 30, 40, and 50) catalysts in the catalytic cracking of C_5 raffinate to light olefins performed at 500 ^{o}C after a 3 h-catalytic reaction, plotted as a function of carbon template content.

3.2.5. Effect of mesoporosity of C(X)-ZSM-5 (X=0, 10, 20, 30, 40, and 50) catalysts on the catalytic activity

We attempted to correlate the mesopore/micropore volume ratio with the catalytic cracking activity of C(X)-ZSM-5 catalysts. Fig. 3.14 showed the correlations between mesopore/micropore volume ratio and catalytic performance of C(X)-ZSM-5 catalysts in the catalytic cracking of C_5 raffinate. The correlations clearly show that catalytic performance of C(X)-ZSM-5 catalysts was closely related to the mesoporosity of the catalysts. Conversion of C_5 raffinate and yield for light olefins increased with increasing mesopore/micropore volume ratio of the catalysts. Therefore, it is believed that the improved catalytic performance of C(X)-ZSM-5 catalysts was attributed to the enhanced mesoporosity of the catalyst. With increasing mesoporosity of the catalyst, reactants were more readily introduced into the active sites of the catalyst, leading to a superior catalytic performance. However, selectivity for ethylene and propylene was not significantly influenced by mesoporosity of the catalyst. That is, selectivity for ethylene and propylene was almost constant with respect to mesoporosity of the catalysts (Fig. 3.13). It has been reported that cracking of hydrocarbon generally occurs through two pathways; monomolecular cracking and bimolecular cracking [73]. Bimolecular cracking is a classical chain process involving hydride transfer from olefins to carbenium intermediate species to form large hydrocarbons. Here, acid sites of the catalyst serve as active sites for both oligomerization and cracking. Stable and constant selectivity for light

olefins may be due to the balance between these two reactions [70]. The simultaneous process of oligomerization for consuming light olefins and cracking for producing light olefins gives rise to constant selectivity for ethylene and propylene. Therefore, it is concluded that mesoporosity of the catalyst played an important role in determining the catalytic performance. Thus, C(X)-ZSM-5 catalysts served as an efficient catalyst in the production of light olefins through catalytic cracking of C_5 raffinate.

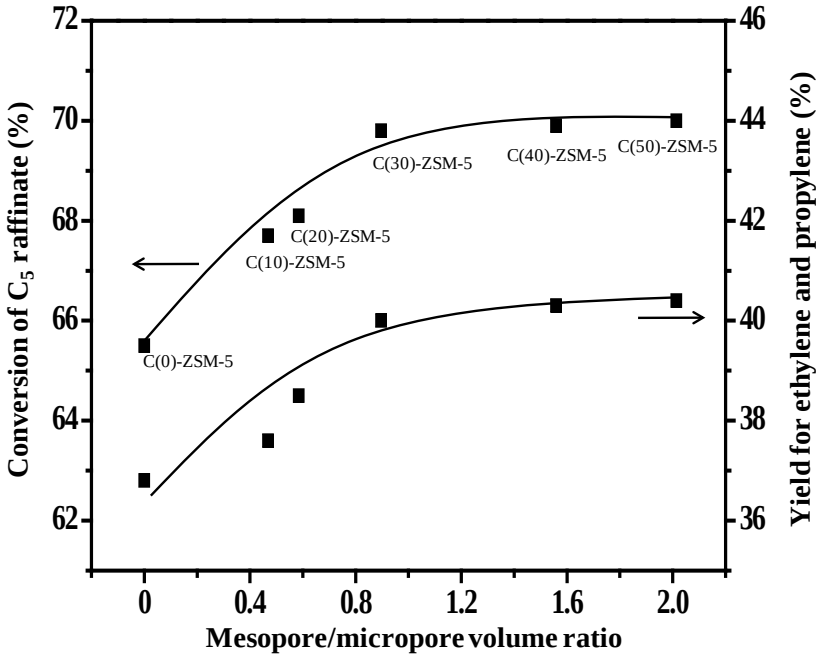

Fig. 3.14. Correlations between mesopore/micropore volume ratio and catalytic performance of C(X)-ZSM-5 (X=0, 10, 20, 30, 40, and 50) catalysts.

3.3. Characterization and catalytic activity of phosphorous modified micro/mesoporous ZSM-5 catalysts

3.3.1. Characterization of phosphorous modified micro/mesoporous ZSM-5 catalysts

Textural property of C-ZSM5 and XP/C-ZSM5 (X=0.17, 0.3, 0.7, 1.4, and 2.7) catalysts was examined by nitrogen adsorption-desorption isotherm measurements. Fig. 3.15 shows the nitrogen adsorption-desorption isotherms of C-ZSM5 and XP/C-ZSM5 catalysts. All the catalysts exhibited IV-type isotherm with H3-type hysteresis loop, indicating the existence of mesopores. This result indicates that XP/C-ZSM5 catalysts were successfully prepared in this work. It was also observed that pore structure of XP/C-ZSM5 catalysts was still maintained even after the loading of phosphorous.

Phosphorous content of XP/C-ZSM5 (X=0.17, 0.3, 0.7, 1.4, and 2.7) catalysts determined by ICP-AES analysis is listed in Table 3.5. Phosphorous content of XP/C-ZSM-5 catalysts was in good agreement with the designed value, indicating that XP/C-ZSM-5 catalysts were successfully prepared. Detailed textural properties of the catalysts are summarized in Table 3.5. BET surface area and pore volume of the catalysts decreased with increasing phosphorous content, which was attributed to the partial blockage of catalyst pore by phosphorous species during the preparation of XP/C-ZSM5 catalysts. This was well consistent with the fact that phosphorous impregnated on

zeolite formed polymeric phosphates species at the entrance of pore channels, leading to a decrease of surface area and pore volume.

Fig. 3.16 shows the XRD patterns of C-ZSM5 and XP/C-ZSM5 (X=0.17, 0.3, 0.7, 1.4, and 2.7) catalysts. All the catalysts showed the intrinsic crystalline structure of ZSM-5, and no additional phase was observed [63]. However, phosphorous-modified XP/C-ZSM5 catalysts exhibited slightly weak peak intensity compared to phosphorous-free C-ZSM5, indicating that crystallinity of the catalyst decreased with increasing phosphorous content. This is because defect sites were generated at the framework of the catalysts during the preparation of XP/C-ZSM5 catalysts due to the partial dealumination. Dealumination dominantly occurred with increasing phosphorous content.

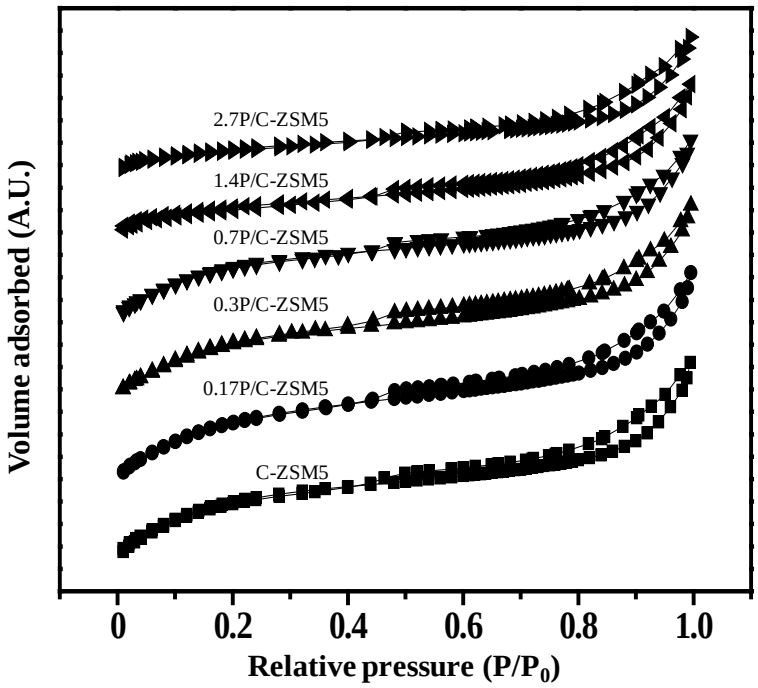

Fig. 3.15. Nitrogen adsorption-desorption isotherms of C-ZSM5 and XP/C-ZSM5 (X=0.17, 0.3, 0.7, 1.4, and 2.7) catalysts.

Table 3.5

Chemical and physical properties of C-ZSM5 and XP/C-ZSM-5 (X=0.17, 0.3, 0.7, 1.4, and 2.7) catalysts

Catalyst	Phosphorous content (wt%) [a]	Surface area (m^2/g) [b]	Pore volume (cm^3/g) [c]	
			Micropore	Mesopore
C-ZSM5	-	396.4	0.146	0.131
0.17P/C-ZSM5	0.17	391.6	0.138	0.128
0.3P/C-ZSM5	0.3	387.8	0.130	0.122
0.7P/C-ZSM5	0.7	384.7	0.121	0.118
1.4P/C-ZSM5	1.4	368.5	0.109	0.116
2.7P/C-ZSM5	2.7	346.7	0.105	0.114

[a] Determined by ICP-AES measurement
[b] Calculated by BET (Brunauer-Emmett-Teller) equation
[c] BJH (Barret-Joyner-Hallender) desorption pore volume

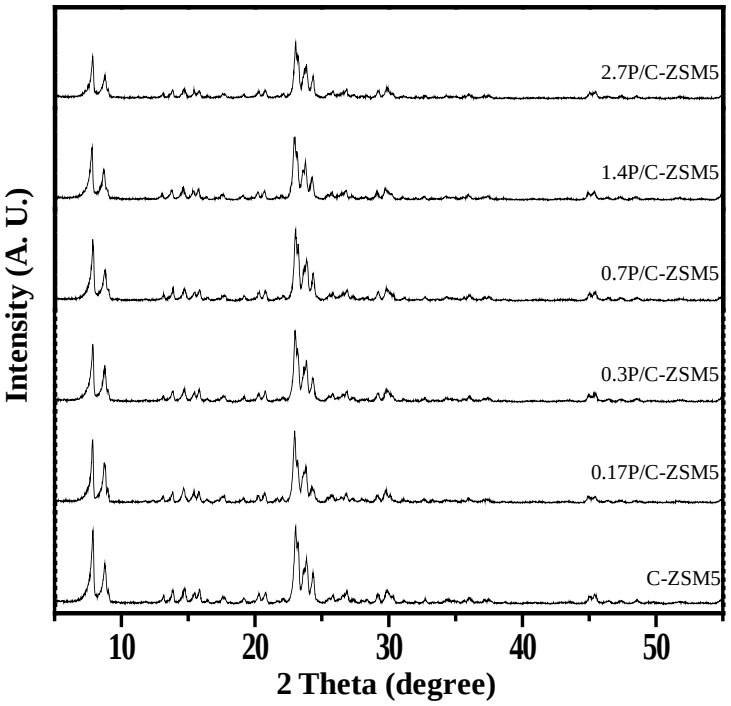

Fig. 3.16. XRD patterns of C-ZSM5 and XP/C-ZSM5 (X=0.17, 0.3, 0.7, 1.4, and 2.7) catalysts.

3.3.2. Acid property of phosphorous modified micro/mesoporous ZSM-5 catalysts

It has been reported that the bridging hydroxyl group of zeolite reflects the acid property of zeolite [74]. Therefore, FT-IR experiments were carried out to see the changes in acidity of C-ZSM5 catalyst after phosphorous modification. Fig. 3.17 shows the FT-IR spectra of C-ZSM5, 0.3P/C-ZSM5, and 1.4P/C-ZSM5 catalysts within the range of 3900-3400 cm^{-1}. The characteristic IR bands of C-ZSM5, 0.3P/C-ZSM5, and 1.4P/C-ZSM5 catalysts appeared at 3740, 3665, and 3603 cm^{-1}, corresponding to non-acidic external silanol group, hydroxyl group bonded to extra-framework alumina, and acidic bridging hydroxyl, respectively [75]. The intensity of these bands decreased with increasing the amount of phosphorous. This result indicates that phosphoric acid introduced into C-ZSM5 interacted with both acidic and non-acidic hydroxyl groups. Furthermore, it can be inferred that the decrease in peak intensity at 3603 cm^{-1} after phosphorous modification was attributed to the interaction between strong acid sites and phosphorous species, resulting in the decrease of strong acidity of XP/C-ZSM5 catalysts.

NH_3-TPD experiments were conducted to determine the acid property of fresh (C-ZSM5 and XP/C-ZSM5 (X=0.17, 0.3, 0.7, 1.4, and 2.7)) and hydrothermal treated (C-ZSM5-St. and XP/C-ZSM5-St. (X=0.17, 0.3, 0.7, 1.4, and 2.7) catalysts. Fig. 3.18 shows the NH_3-TPD profiles of fresh (C-ZSM5 and XP/C-ZSM5) and hydrothermal treated (C-ZSM-St. and XP/C-ZSM5-St.) catalysts. Acidity of catalysts determined from TPD peak area is summarized

in Table 3.6. It was found that weak acidity of the catalysts was not significantly changed after phosphorous modification in the fresh catalysts. However, strong acidity of the catalysts decreased with increasing phosphorous content. As a consequence, total acidity of the catalysts decreased with increasing phosphorous content, indicating that acidity of the catalyst was strongly affected by phosphorous content. After hydrothermal treatment of fresh catalysts, all the samples sharply reduced the acidity. This is because dealumination of the fresh catalysts occurred during hydrothermal treatment causing decrease in acid sites. However, phosphorous modified XP/C-ZSM5 reserved more acid sites compared to the pure C-ZSM5 catalyst after hydrothermal treatment. It can be assumed that phosphorous introduced in C-ZSM5 catalyst inhibited the dealumination of the catalyst by hydrothermal treatment and preserving acid sites.

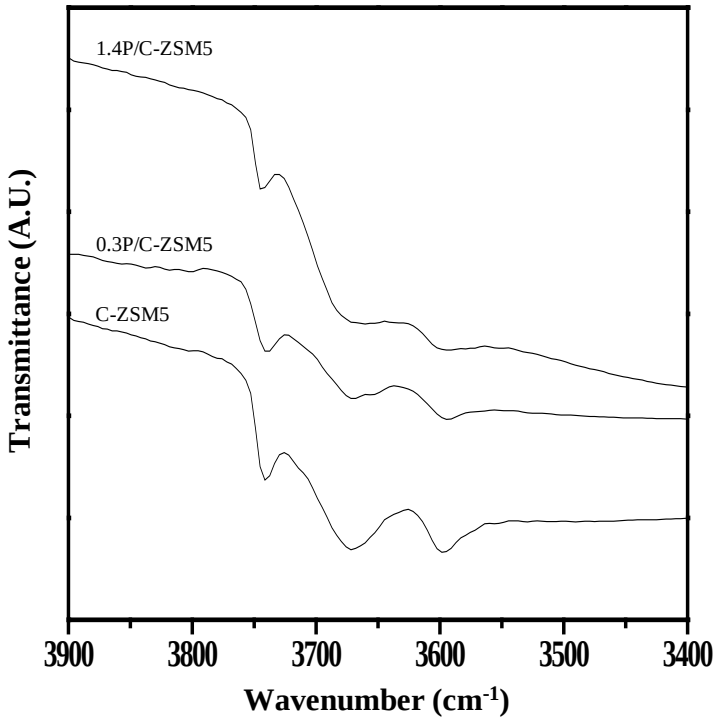

Fig. 3.17. FT-IR spectra of C-ZSM5, 0.3P/C-ZSM5, and 1.4P/C-ZSM5 catalysts.

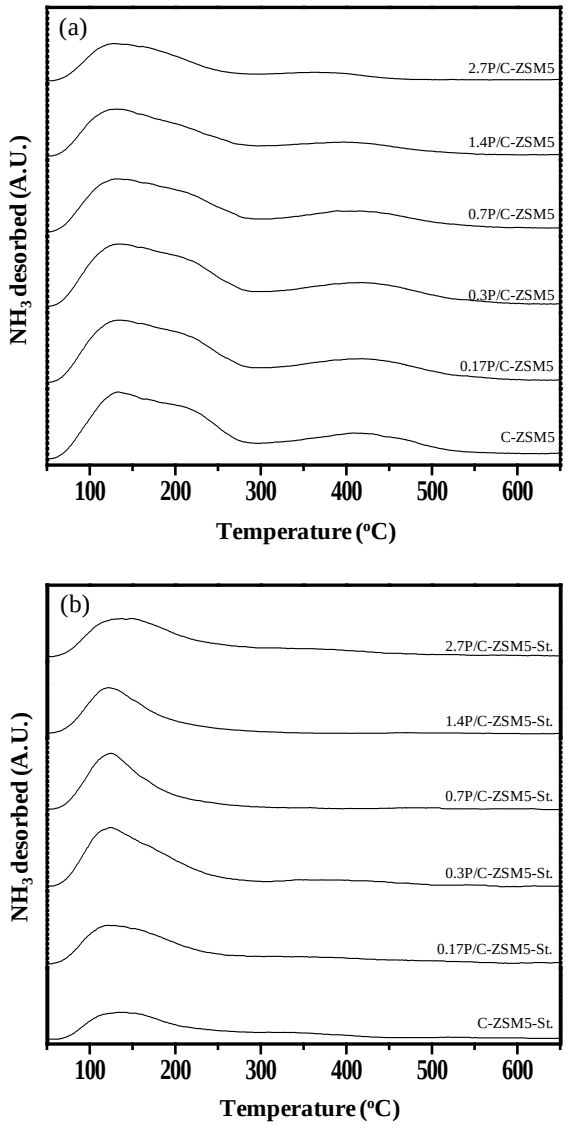

Fig. 3.18. NH_3-TPD profiles of (a) fresh (C-ZSM5 and XP/C-ZSM5 (X=0.17, 0.3, 0.7, 1.4, and 2.7)) and (b) hydrothermal treated (C-ZSM5-St. and XP/C-ZSM5-St. (X=0.17, 0.3, 0.7, 1.4, and 2.7) catalysts.

Table 3.6

Acidity of (a) fresh (C-ZSM5 and XP/C-ZSM5 (X=0.17, 0.3, 0.7, 1.4, and 2.7)) and (b) hydrothermal treated (C-ZSM5-St. and XP/C-ZSM5-St. (X=0.17, 0.3, 0.7, 1.4, and 2.7) catalysts

Catalyst	Acidity (mmol-NH_3/g)
C-ZSM5	139.5
0.17P/C-ZSM5	134.7
0.3P/C-ZSM5	127.9
0.7P/C-ZSM5	114.1
1.4P/C-ZSM5	102.6
2.7P/C-ZSM5	92.3
C-ZSM5-St.	73.3
0.17P/C-ZSM5-St.	88.2
0.3P/C-ZSM5-St.	104.5
0.7P/C-ZSM5-St.	98.6
1.4P/C-ZSM5-St.	93.3
2.7P/C-ZSM5-St.	86.4

3.3.3. Effect of hydrothermal treatment on aluminum chemical states of the phosphorous modified micro/mesoporous ZSM-5 catalysts

^{27}Al MAS NMR analyses were conducted in order to investigate the chemical states of aluminum species in the catalysts. As shown in Fig. 3.19 (a), C-ZSM5 catalyst exhibited a peak at 54 ppm along with a weak peak at 0 ppm. The peaks at 55 and 0 ppm correspond to tetrahedrally coordinated aluminum in the zeolite framework and octahedrally coordinated aluminum in the extra framework, respectively [76,77]. It was found that the peak intensity at 54 ppm decreased with increasing phosphorous content, and the peak at 0 ppm almost disappeared after phosphorous modification. On the other hand, a new peak at -9 ppm assigned to octahedral aluminum attached to phosphorous atom (aluminum phosphate), which prevented migration of aluminum atoms to extra framework position under severe reaction conditions, was observed in the 0.3P/C-ZSM5 and 1.4P/C-ZSM5 catalysts. It is generally accepted that strong acid sites are relate to the tetrahedral coordinated aluminum (54 ppm) in zeolite [50]. Therefore, it can be inferred that a decrease in peak intensity at 54 ppm indicates decrement of strong acid sites after phosphorous modification, and this result is well consistent with NH_3-TPD and FT-IR results.

Fig. 3. 19 (b) showed the ^{27}Al MAS NMR analyses results of hydrothermal treated C-ZSM5-St., 0.3P/C-ZSM5-St., and 1.4P/C-ZSM5-St. catalysts. all the hydrothermal treated catalysts exhibited weaker peak

intensity at 55 ppm compared with fresh catalysts, indicating decrease in framework aluminum caused by dealumination during the hydrothermal treatment. It was found that phosphorous free C-ZSM5-St. catalyst was more readily dealuminated compared with phosphorous modified 0.3P/C-ZSM5-St. and 1.4P/C-ZSM5-St. catalysts. Furthermore, it was observed that C-ZSM5-St. catalyst generated octahedral coordinated aluminum, while 0.3P/C-ZSM5-St. and 1.4P/C-ZSM5-St. catalysts mainly formed aluminum phosphates. Although phosphorous modification also leads partial dealumination of the catalyst, modification of C-ZSM5 catalyst with phosphorous prevents some extension of dealumination of the catalyst during the hydrothermal treatment by formation of aluminum phosphates, which prevent migration of framework aluminum atoms to extra-framework positions [76].

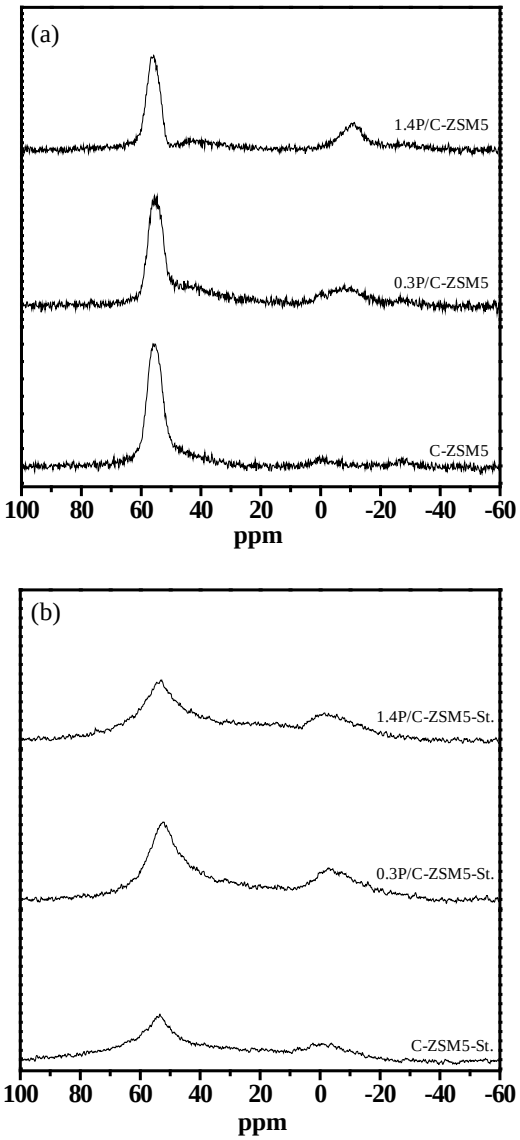

Fig. 3.19. ^{27}Al MAS NMR spectra of (a) C-ZSM5, 0.3P/C-ZSM5, and 1.4P/C-ZSM5 catalysts and (b) C-ZSM5-St., 0.3P/C-ZSM5-St., and 1.4P/C-ZSM5-St. catalysts.

3.3.4. Catalytic activity of phosphorous modified phosphorous modified micro/mesoporous ZSM-5 catalysts

Fig. 3.20 shows the catalytic performance of fresh catalyst (C-ZSM5 and XP/C-ZSM5 (X=0.17, 0.3, 0.7, 1.4, and 2.7)) and steamed catalyst (C-ZSM5-St. and XP/C-ZSM5-St. (*X*=0.17, 0.3, 0.7, 1.4, and 2.7)) in the catalytic cracking of C_5 raffinate to light olefins (ethylene and propylene) performed at 600 ^{o}C after a 3 h-catalytic reaction. It is interesting to note that catalytic performance of the prepared catalysts was quite different before and after hydrothermal treatment. C-ZSM5 catalyst exhibited a highest C_5 raffinate conversion and yield for light olefins before hydrothermal treatment, and catalytic activities decreased with increasing phosphorous content in the XP/C-ZSM5 catalyst.

It was found that all the hydrothermal treated catalysts exhibited lower catalytic activity than fresh catalyst, which was attributed to the dealumination of the catalyst during the hydrothermal treatment. In particular, hydrothermal treated C-ZSM5-St. catalyst exhibited significant decrease in catalytic activity, indicating that C-ZSM5-St. catalyst was less hydrothermally stable than phosphorous containing XP/C-ZSM5-St. catalysts. Conversion of C_5 raffinate and yield for light olefins showed volcano-shaped trend with respect to phosphorous content. This result indicates that phosphorous modification improves hydrothermal stability of the catalyst by preventing segregation of the framework aluminum atoms. Among the catalyst tested, 0.3P/C-ZSM5-St. catalysts showed best catalytic performance in terms of

conversion of C_5 raffinate and yield for light olefins. When phosphorous content is larger than 0.3 wt%, however, no enhancement in the catalytic activity was found even though those catalysts were also hydrothermally stable. This is because large amount of phosphorous containing catalyst cause diffusional problem of reactants and products due to the micropore blockage by phosphorous species (Table 3.5), and significant decrease in acidity of the catalysts also leads low catalytic activity. Therefore, it is concluded that optimal amount of phosphorous content was required for the maximum production of light olefin through catalytic cracking of C_5 raffinate, and in turn, phosphorous modification of ZSM-5 served as an effect method to improve the hydrothermal stability of the catalyst.

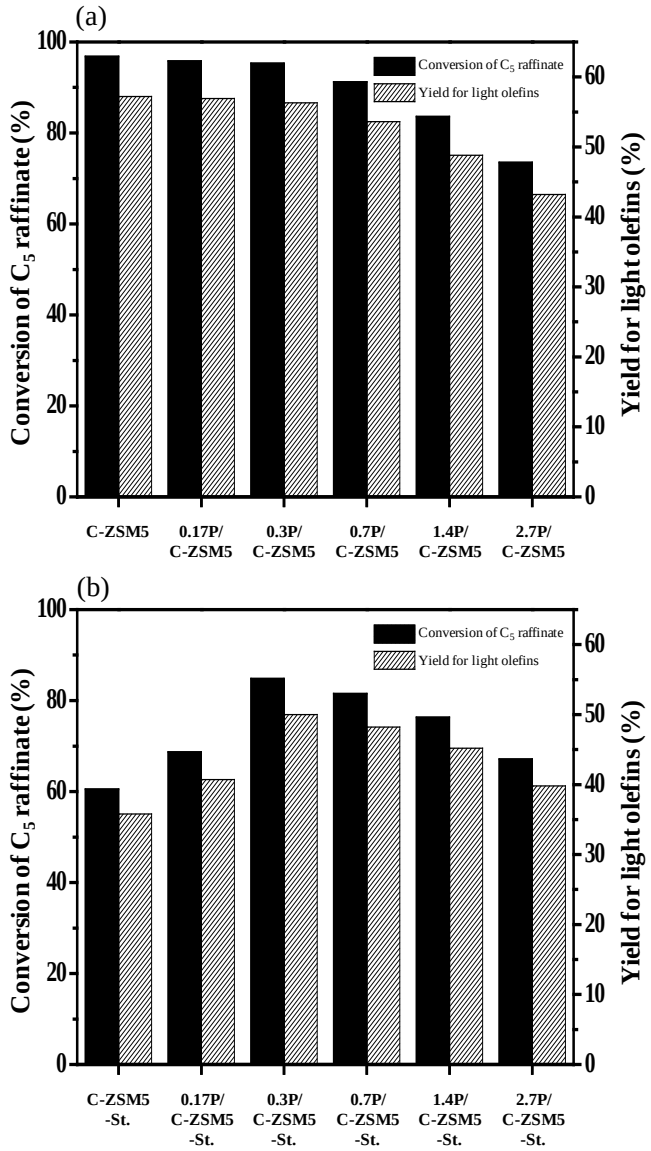

Fig. 3.20. Catalytic performance of (a) fresh catalysts (C-ZSM5 and XP/C-ZSM5 (X=0.17, 0.3, 0.7, 1.4, and 2.7)) and (b) steamed catalyst (C-ZSM5-St. and *X*P/C-ZSM5-St. (*X*=0.17, 0.3, 0.7, 1.4, and 2.7)) in the catalytic cracking of C_5 raffinate to light olefins.

3.4. Characterization and catalytic activity of lanthanum-containing phosphorous modified micro/mesoporous ZSM-5 catalysts

3.4.1. Characterization of lanthanum-containing phosphorous modified micro/mesoporous ZSM-5 catalysts

Fig. 3.21 shows the XRD patterns of LaX-P/C-ZSM5 (X=0.3, 0.7, 0.9, and 1.2) catalysts. For comparison, XRD pattern of P/C-ZSM5 catalyst is also presented in Fig. 3.21. All the catalysts exhibited an intrinsic crystalline structure of ZSM-5, indicating that LaX-P/C-ZSM5 catalysts were successfully prepared without any loss of MFI structure even after the introduction of lanthanum [63]. Compared to P/C-ZSM5 catalyst, however, LaX-P/C-ZSM5 catalysts showed weak peak intensity at low angle ($2\theta < 10^{o}$) and the peak intensity gradually decreased with increasing lanthanum content. It is known that XRD peak intensity of ZSM-5 at low angle is sensitive to the presence of any metal species inside the channel of ZSM-5 [78]. Therefore, it can be inferred that the decrease of peak intensity of LaX-P/C-ZSM5 catalysts at low angle was attributed to the existence of lanthanum species inside the channel of P/C-ZSM5. It was also found that no additional diffraction peaks corresponding to lanthanum species were observed in the LaX-P/C-ZSM5 catalysts. This indicates that lanthanum species were finely dispersed on the surface of P/C-ZSM5 or penetrated into the channel of P/C-ZSM5 as fine

particles.

Textural property of P/C-ZSM5 and LaX-P/C-ZSM5 (X=0.3, 0.7, 0.9, and 1.2) catalysts was examined by nitrogen adsorption-desorption isotherm measurements. Fig. 3.22 shows the nitrogen adsorption-desorption isotherms of P/C-ZSM5 and LaX-P/C-ZSM5 catalysts. It was observed that all the catalysts exhibited IV-type isotherm with H3-type hysteresis loop, indicating the existence of mesopores. This result supports that porous C-ZSM5 was successfully prepared.

Detailed chemical and physical properties of P/C-ZSM5 and LaX-P/C-ZSM5 (X=0.3, 0.7, 0.9, and 1.2) catalysts are summarized in Table 3.7. BET surface area and pore volume of the catalysts decreased with increasing lanthanum content. This is attributed to the partial blockage of catalyst pore by lanthanum species during the preparation of LaX-P/C-ZSM5 catalysts. It is noteworthy that micropore volume of LaX-P/C-ZSM5 catalysts significantly decreased with increasing lanthanum content compared to mesopore volume. This implies that micropore rather than mesopore of the catalyst was readily blocked by additional lanthanum species. Thus, the use of mesoporous ZSM-5 can be an efficient strategy to reduce pore blockage which frequently occurs in the modification of ZSM-5 with various metals. The measured La/Al atomic ratios of LaX-P/C-ZSM5 catalysts were in good agreement with the designed values, indicating that LaX-P/C-ZSM5 catalysts were successfully prepared as attempted in this work.

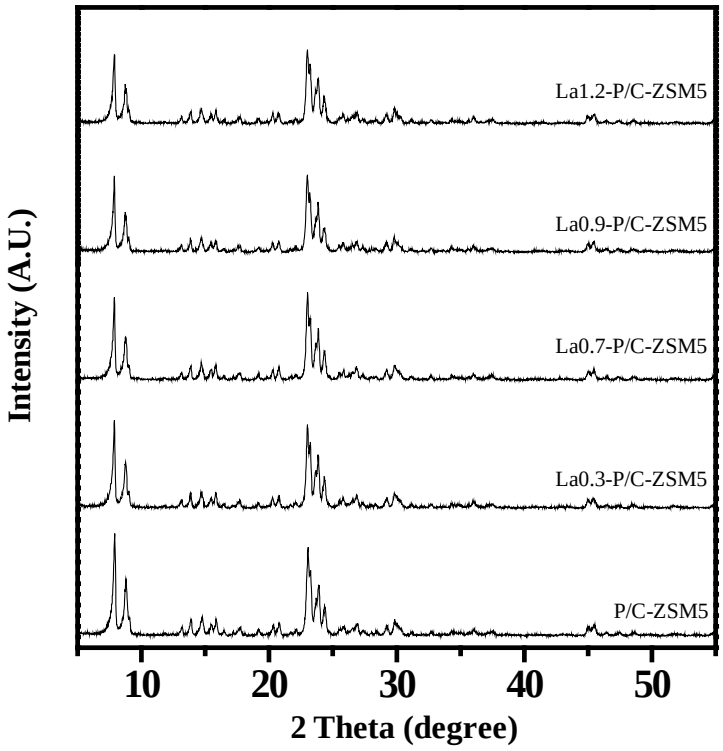

Fig. 3.21. XRD patterns of P/C-ZSM5 and LaX-P/C-ZSM5 (X=0.3, 0.7, 0.9, and 1.2) catalysts.

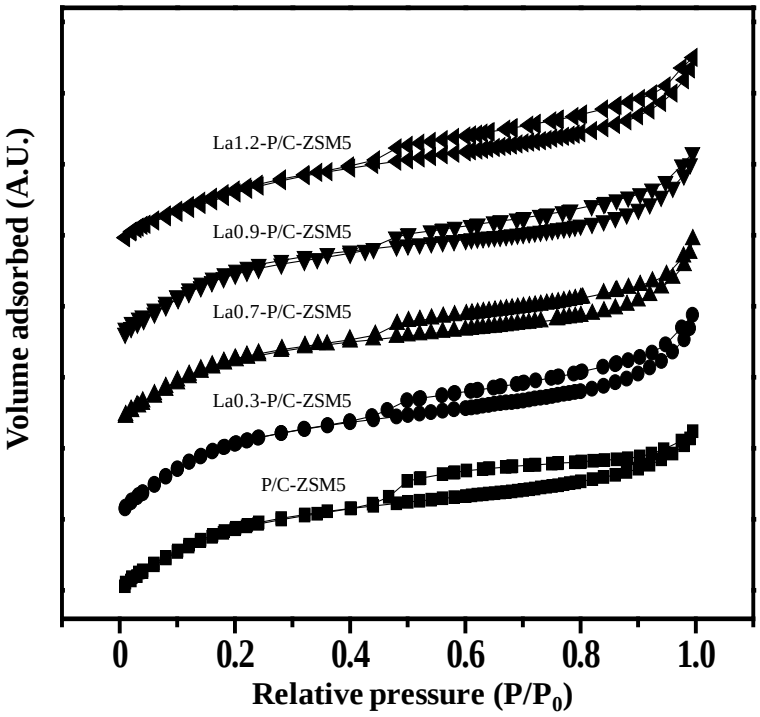

Fig. 3.22. Nitrogen adsorption-desorption isotherms of P/C-ZSM5 and LaX-P/C-ZSM5 (X=0.3, 0.7, 0.9, and 1.2) catalysts.

Table 3.7

Chemical and physical properties of P/C-ZSM5 and LaX-P/C-ZSM5 (X=0.3, 0.7, 0.9, and 1.2) catalysts.

Catalyst	La/Al atomic ratio [a]	Surface area (m^2/g) [b]	Pore volume (cm^3/g) [c]	
			Micropore	Mesopore
P/C-ZSM5	-	387.8	0.148	0.114
La0.3-P/ C-ZSM5	0.27	384.2	0.131	0.109
La0.7-P/ C-ZSM5	0.68	368.7	0.123	0.108
La0.9-P/ C-ZSM5	0.91	360.3	0.115	0.102
La1.2-P/ C-ZSM5	1.23	312.2	0.111	0.097

[a] Determined by ICP-AES measurement
[b] Calculated by BET (Brunauer-Emmett-Teller) equation
[c] BJH (Barret-Joyner-Hallender) desorption pore volume

3.4.2. Catalytic activity of lanthanum-containing phosphorous modified micro/mesoporous ZSM-5 catalysts

Fig. 3.23 shows the catalytic performance of P/C-ZSM5 and LaX-P/C-ZSM5 (X=0.3, 0.7, 0.9, and 1.2) catalysts in the production of light olefins through catalytic cracking of C_5 raffinate at 600 ^oC after a 3 h-catalytic reaction. It was found that conversion of C_5 raffinate decreased with increasing lanthanum content. Selectivity for light olefins (ethylene + propylene) gradually increased with increasing lanthanum content, while selectivity for BTX (benzene, toluene, and xylene) gradually decreased with increasing lanthanum content. As a consequence, yield for light olefins exhibited a volcano-shaped trend with respect to lanthanum content. Among the catalyst tested, La0.7-P/C-ZSM5 catalyst showed the best catalytic performance in terms of yield for light olefins.

It has been reported that hydrogen transfer activity of the catalyst serves as an important factor determining the product distribution in the catalytic cracking of hydrocarbons [79-81]. The catalyst with high hydrogen transfer activity promotes cyclization and aromatization of primary products to form aromatics. On the other hand, the catalyst with low hydrogen transfer activity prevents secondary bimolecular reaction between primary products and carbenium ions through a hydrogen transfer reaction, suppressing the formation of aromatics and enhancing the formation of light olefins. Therefore, it is important to design a catalyst with low hydrogen transfer activity to increase light olefin selectivity. Hydrogen transfer coefficient,

which reflects hydrogen transfer activity of the catalyst, was obtained in this work as listed in Table 3.8. Hydrogen transfer coefficient was defined as the ratio of butanes with respect to butenes (($iC_4 + nC_4$)/$\Sigma C_4^=$) [82,83] which were produced after the reaction. It was found that hydrogen transfer coefficient of LaX-P/C-ZSM5 (X=0.3, 0.7, 0.9, and 1.2) catalysts decreased with increasing lanthanum content. Thus, hydrogen transfer activity of LaX-P/C-ZSM5 catalysts was strongly influenced by lanthanum content.

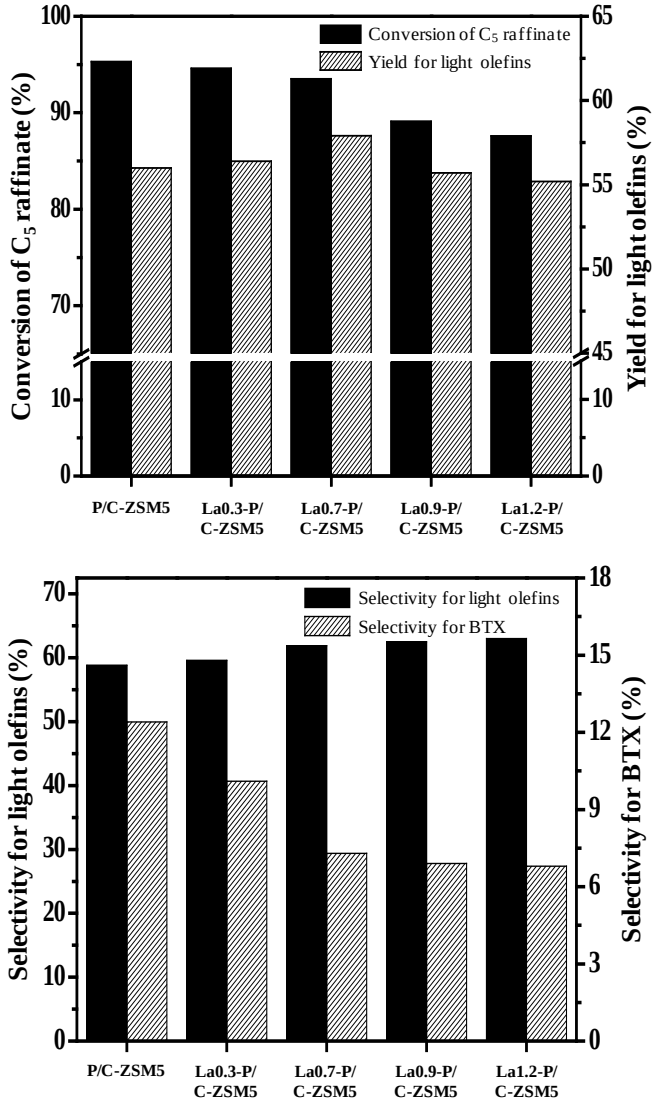

Fig. 3.23. Catalytic performance of P/C-ZSM5 and LaX-P/C-ZSM5 (X=0.3, 0.7, 0.9, and 1.2) catalysts in the catalytic cracking of C_5 raffinate at 600 ^oC after a 3 h-catalytic reaction.

Table 3.8

Hydrogen transfer coefficient of P/C-ZSM5 and LaX-P/C-ZSM5 (X=0.3, 0.7, 0.9, and 1.2) catalysts

Catalyst	Hydrogen transfer coefficient
P/C-ZSM5	0.55
La0.3-P/C-ZSM5	0.47
La0.7-P/C-ZSM5	0.40
La0.9-P/C-ZSM5	0.34
La1.2-P/C-ZSM5	0.31

3.4.3. Acid property of lanthanum-containing phosphorous modified micro/mesoporous ZSM-5 catalysts

NH_3-TPD experiments were conducted to determine the acid property of P/C-ZSM5 and LaX-P/C-ZSM5 (X=0.3, 0.7, 0.9, and 1.2) catalysts. Fig. 3. 24 shows the NH_3-TPD profiles of P/C-ZSM5 and LaX-P/C-ZSM5 catalysts. All the catalysts showed two major desorption peaks at around 130 ^oC and 390 ^oC corresponding to weak acid site and strong acid site, respectively. Acidity of P/C-ZSM5 and LaX-P/C-ZSM5 catalysts determined from TPD peak area is summarized in Table 3.9. Although acid strength of LaX-P/C-ZSM5 catalysts was not changed after the introduction of lanthanum, acidity of the catalysts was strongly influenced by lanthanum content. It was found that both weak acidity and strong acidity of LaX-P/C-ZSM5 catalysts decreased with increasing lanthanum content. As a consequence, total acidity of the catalysts decreased with increasing lanthanum content.

FT-IR experiments were conducted to see the changes in acidity of P/C-ZSM5 catalysts after the introduction of lanthanum. Fig. 3.25 shows the FT-IR spectra of P/C-ZSM5, La0.7-P/C-ZSM5, and La1.2-P/C-ZSM5 catalysts within the range of 3800-3500 cm^{-1}. All the measured catalysts exhibited the characteristic IR bands at 3740, 3665, and 3603 cm^{-1}, corresponding to non-acidic external silanol group, hydroxyl group bonded to extra-framework alumina, and acidic bridging hydroxyl group, respectively [75]. It was found that intensity of these bands decreased with increasing lanthanum content. This result indicates that lanthanum introduced into P/C-ZSM5 catalyst

interacted with both acidic and non-acidic hydroxyl groups. The decrease in acidity after the addition of lanthanum into P/C-ZSM5 was attributed to the consumption of acid sites by lanthanum species. When lanthanum was introduced into P/C-ZSM5, it preferentially interacted with acidic hydroxyl groups of P/C-ZSM5, resulting in the decrease of acidity of LaX-P/C-ZSM5 catalysts, as demonstrated in NH_3-TPD results.

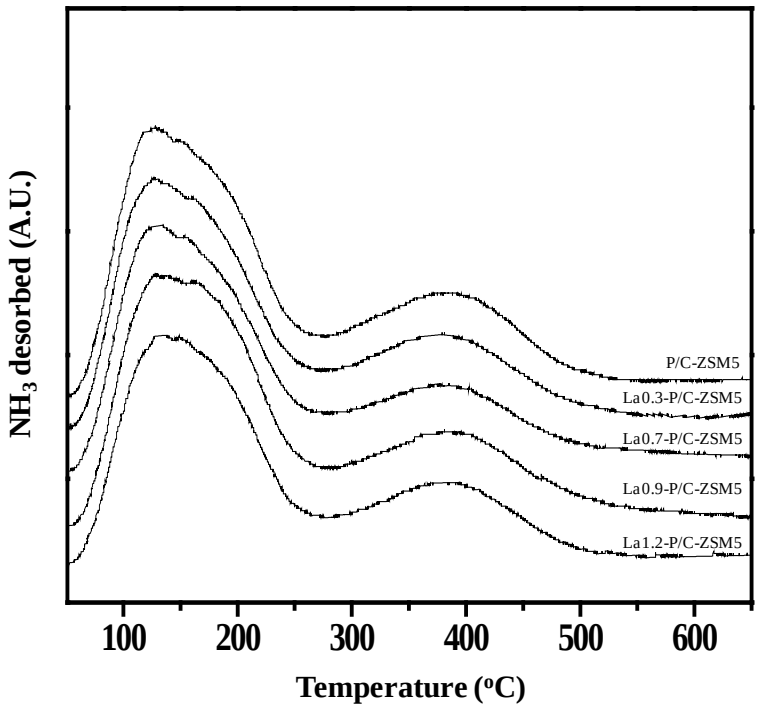

Fig. 3.24. NH_3-TPD profiles of P/C-ZSM5 and LaX-P/C-ZSM5 (X=0.3, 0.7, 0.9, and 1.2) catalysts.

Table 3.9

Acidity of P/C-ZSM5 and LaX-P/C-ZSM5 (X=0.3, 0.7, 0.9, and 1.2) catalysts

Catalyst	Acidity (μmol-NH_3/g)
P/C-ZSM5	125.6
La0.3-P/C-ZSM5	122.5
La0.7-P/C-ZSM5	119.6
La0.9-P/C-ZSM5	112.1
La1.2-P/C-ZSM5	106.8

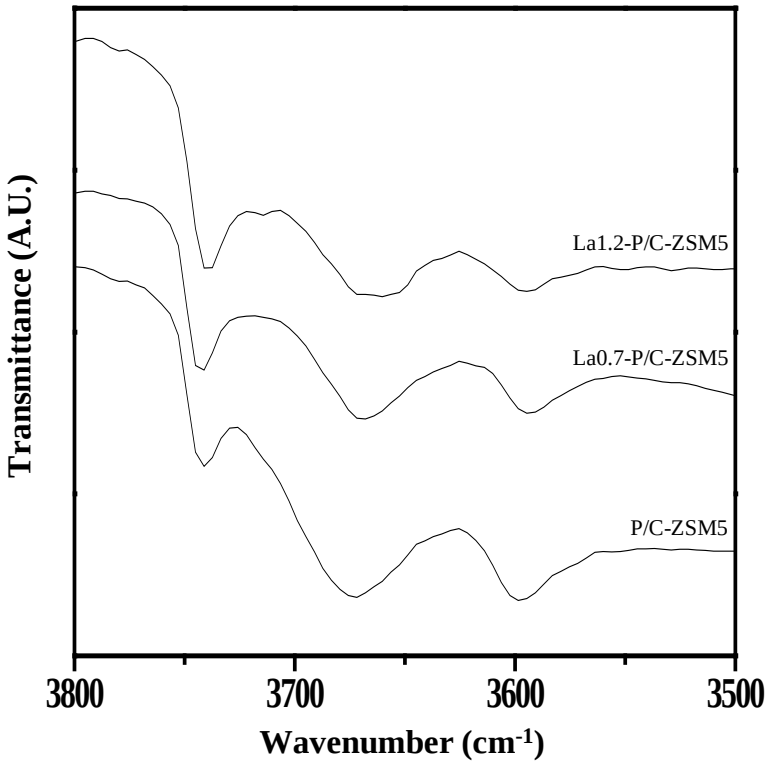

Fig. 3.25. FT-IR spectra of P/C-ZSM5, La0.7-P/C-ZSM5, and La1.2-P/C-ZSM5 catalysts.

3.4.4. Base property of lanthanum-containing phosphorous modified micro/mesoporous ZSM-5 catalysts

It has been reported that lanthanum-loaded ZSM-5 generates basic sites on the external surface of ZSM-5 [84]. Therefore, CO_2-TPD measurements were conducted to investigate the effect of lanthanum content on the basicity of LaX-P/C-ZSM5 (X=0.3, 0.7, 0.9, and 1.2) catalysts. Fig. 3.26 shows the CO_2-TPD profiles of P/C-ZSM5 and LaX-P/C-ZSM5 catalysts. Basicity of P/C-ZSM5 and LaX-P/C-ZSM5 catalysts calculated from the peak area is summarized in Table 3.10. It was found that basicity of LaX-P/C-ZSM5 catalysts was significantly different with a variation of lanthanum content. Basicity of LaX-P/C-ZSM5 catalysts increased with increasing lanthanum content.

In the bimolecular cracking mechanism, hydrogen transfer reaction generally occurs not only between reactant and adsorbed carbenium ions but also between primary products and adsorbed carbenium ions. An important point determining the hydrogen transfer activity is how many primary products are readsorbed and participate in the hydrogen transfer reaction. The basicity of the catalyst inhibiting the readsorption of primary products during the reaction, therefore, can be a crucial factor determining the hydrogen transfer activity. Fig. 3.27 shows the relationship between basicity and hydrogen transfer coefficient of LaX-P/C-ZSM5 catalysts. It was observed that hydrogen transfer coefficient was closely related to the basicity of LaX-P/C-ZSM5 catalysts. The hydrogen transfer coefficient decreased with

increasing basicity of the catalyst. This is because base sites of LaX-P/C-ZSM5 catalysts inhibited the readsorption of primarily produced olefins, preventing hydrogen transfer reaction between carbenium ions and readsorbed olefins.

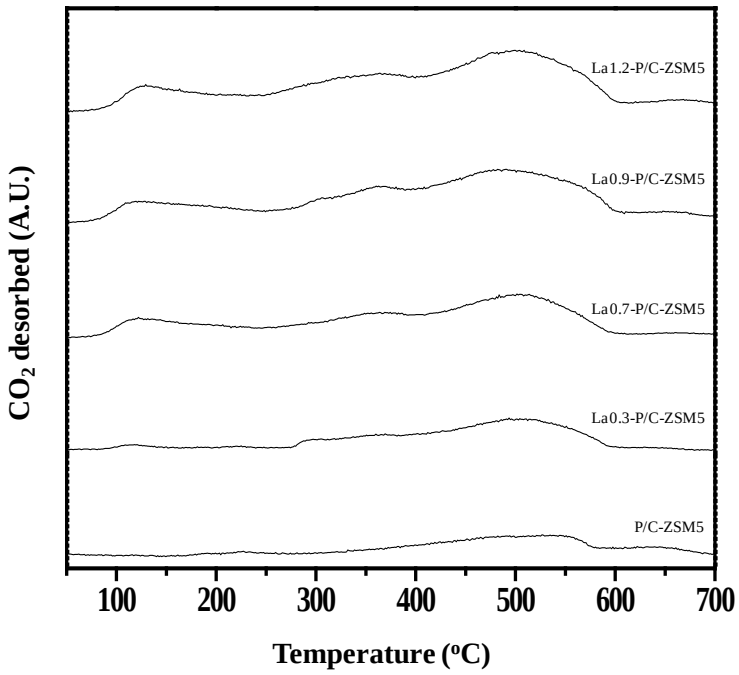

Fig. 3.26. CO_2-TPD profiles of P/C-ZSM5 and LaX-P/C-ZSM5 (X=0.3, 0.7, 0.9, and 1.2) catalysts.

Table 3.10

Basicity of P/C-ZSM5 and LaX-P/C-ZSM5 (X=0.3, 0.7, 0.9, and 1.2) catalysts

Catalyst	Basicity (μmol-CO_2/g)
P/C-ZSM5	5.8
La0.3-P/C-ZSM5	6.9
La0.7-P/C-ZSM5	12.2
La0.9-P/C-ZSM5	13.8
La1.2-P/C-ZSM5	21.1

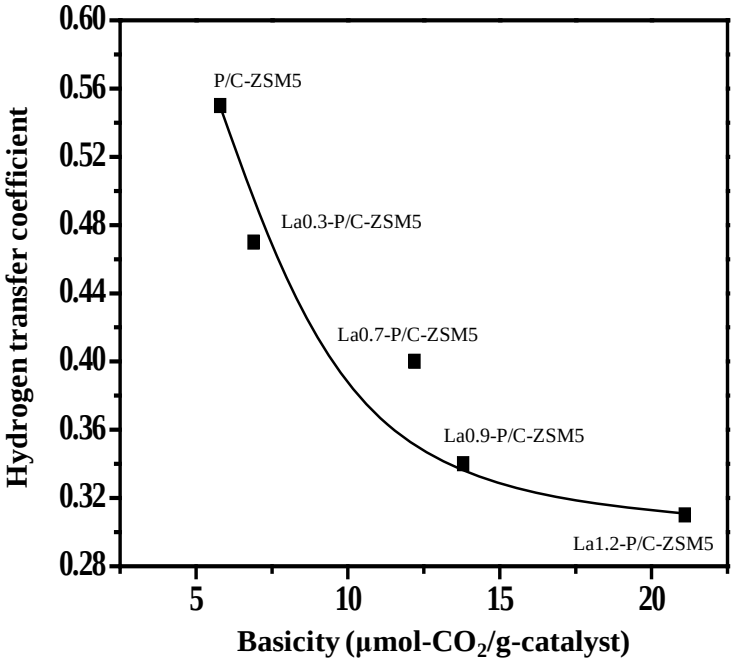

Fig. 3.27. Relationship between basicity and hydrogen transfer coefficient of P/C-ZSM5 and LaX-P/C-ZSM5 (X=0.3, 0.7, 0.9, and 1.2) catalysts.

3.4.5. Effect of acidity and basicity on the catalytic performance

It has been reported that acidity of the catalyst is one of the crucial factors determining the catalytic performance in the catalytic cracking of hydrocarbons [67]. Thus, an attempt has been made to correlate acidity with catalytic performance of P/C-ZSM5 and LaX-P/C-ZSM5 (X=0.3, 0.7, 0.9, and 1.2) catalysts. Fig. 3.28 (a) shows the correlation between acidity and conversion of C_5 raffinate over P/C-ZSM5 and LaX-P/C-ZSM5 catalysts. Conversion of C_5 raffinate decreased with decreasing acidity of the catalyst. It is generally accepted that cracking activity of the catalyst decreases with decreasing acidity of the catalyst [85]. Therefore, the decrease of C_5 raffinate conversion over LaX-P/C-ZSM5 with increasing lanthanum content was mainly due to the decrease of acidity of the catalyst.

It has been reported that selectivity for light olefins was influenced by basicity of the catalyst [7,70]. Fig. 3.28 (b) shows the correlation between basicity and selectivity for light olefins (ethylene + propylene) and BTX. The correlation clearly shows that selectivity for light olefins increased with increasing basicity of the catalyst, while selectivity for BTX decreased with increasing basicity of the catalyst. The increased selectivity for light olefins with increasing basicity of LaX-P/C-ZSM5 catalysts was attributed to the decrease of hydrogen transfer activity (Fig. 3.27). It is known that light olefins, which are primarily produced in the cracking reaction, undergo cyclization and dehydrogenation on the acid sites of the catalyst through hydrogen transfer reaction to form aromatics [67]. Furthermore, aromatics generated by

secondary reaction between olefins and carbenium ions cause coke formation, leading to a catalyst deactivation. Therefore, hydrogen transfer activity of the catalyst should be minimized to enhance light olefin selectivity and to reduce coke formation. As shown in Fig. 3. 28, conversion of C_5 raffinate and selectivity for light olefins over LaX-P/C-ZSM5 (X=0.3, 0.7, 0.9, and 1.2) were closely related to the acid and base properties of the catalyst, respectively. In this work, yield for light olefins was obtained by multiplying conversion of C_5 raffinate and selectivity for light olefins. As a result, maximum catalytic performance in terms of yield for light olefins could be obtained over La0.7-P/C-ZSM5 catalyst, which retained moderate acidity and basicity.

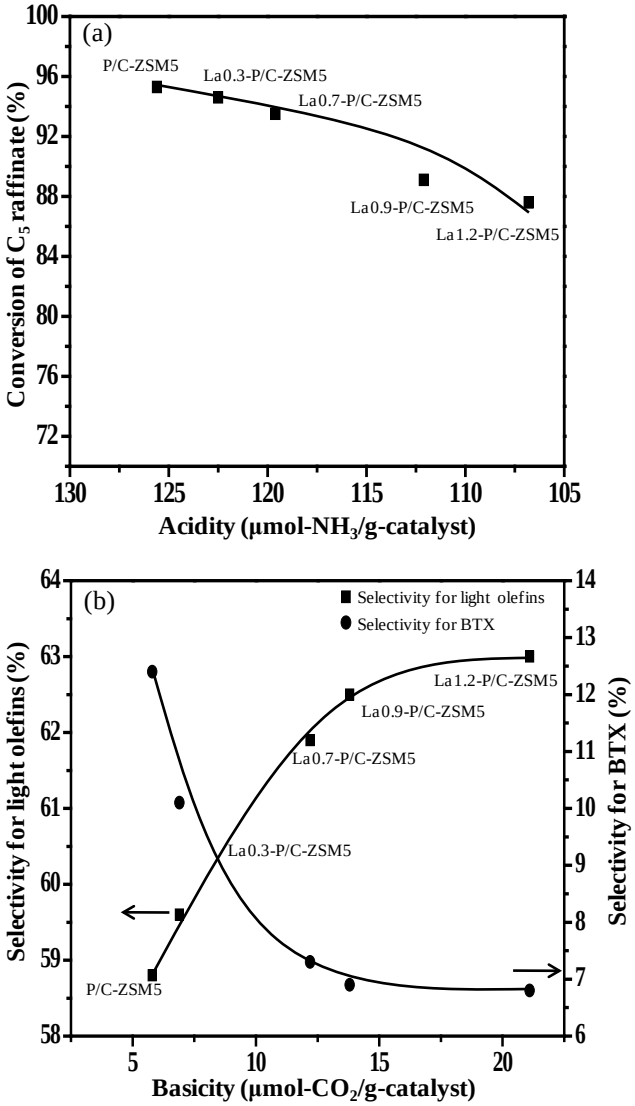

Fig. 3.28. (a) Correlation between acidity and conversion of C_5 raffinate and (b) correlation between basicity and selectivity for light olefins and BTX over P/C-ZSM5 and LaX-P/C-ZSM5 (X=0.3, 0.7, 0.9, and 1.2) catalysts.

Chapter 4. Conclusions

Various modified ZSM-5 catalysts were prepared, including micro/mesoporous featured ZSM-5, phosphorous modified ZSM-5, and lanthanum containing ZSM-5, and they were applied to the light olefin production from catalytic cracking of C_5 raffinate. The effect of modification of ZSM-5 on the physicochemical properties and catalytic performance in the catalytic cracking of C_5 raffinate to light olefins was investigated.

A series of microporous and mesoporous ZSM5 catalysts (PAM(X)-ZSM5) were prepared using polyacrylamide (PAM) as a soft template at different PAM content (X=0, 0.12, 0.25, 0.53, 0.64, and 0.78 wt%). The prepared catalysts were then applied to the production of light olefin (ethylene and propylene) through catalytic cracking of C_5 raffinate. Physicochemical properties of PAM(X)-ZSM5 catalysts were strongly influenced by PAM content. It was found that ZSM5 catalysts with micropores and mesopores were successfully synthesized using PAM template, and mesoporosity of the prepared catalysts was easily controlled by adjusting PAM content. Catalytic performance of PAM(X)-ZSM5 catalysts was closely related to the mesoporosity of the catalysts. Conversion of C_5 raffinate and yield for light olefins showed volcano-shaped curves with respect to mesopore/micropore volume ratio of the catalysts. The improved catalytic performance of PAM(X)-ZSM5 (X=0.12-0.64) catalysts compared to conventional PAM(0)-ZSM5 catalyst was attributed to the enhanced mesoporosity of the catalysts, which accelerated the diffusion of reactants into active sites of the catalysts.

However, PAM(0.78)-ZSM5 catalyst exhibited much lower catalytic activity than the other catalysts due to its low crystallinity and small acidity. Thus, an optimal PAM content was required for the maximum production of light olefins through catalytic cracking of C_5 raffinate.

ZSM-5 catalysts (C(X)-ZSM-5) with micropores and mesopores were prepared by hard templating method using carbon as hard template with a variation of carbon template content (X=0, 10, 20, 30, 40, and 50 wt%). The prepared catalysts were then applied to the production of light olefin (ethylene and propylene) through catalytic cracking of C_5 raffinate. Physicochemical properties of C(X)-ZSM-5 catalysts were strongly influenced by carbon template content. Adsorption ability for n-pentane and mesopore volume of C(X)-ZSM-5 catalysts increased with increasing carbon template content. Catalytic performance of C(X)-ZSM-5 catalysts was closely related to the mesoporosity of the catalyst. Conversion of C_5 raffinate and yield for light olefins increased with increasing mesopore/micropore volume ratio of the catalyst, while selectivity for ethylene and propylene showed constant values. High catalytic performance of C(X)-ZSM-5 catalysts compared to conventional ZSM-5 catalyst was attributed to the enhanced mesoporosity of C(X)-ZSM-5 catalysts, which accelerated the diffusion of reactant into active sites of the catalyst. It is concluded that carbon template content in the C(X)-ZSM-5 catalysts strongly affected the mesoporosity of the catalyst, and in turn, mesoporosity played an important role in determining the catalytic performance in the production of light olefins through catalytic cracking of C_5 raffinate.

In order to enhance the hydrothermal stability of micro/mesoporous

ZSM-5 (C-ZSM-5) catalysts prepared by carbon templating method, phosphorous modification was carried out. A series of phosphorous modified ZSM-5 catalysts (XP/C-ZSM5) with micro/mesoporous nature were prepared with a variation of phosphorous content (X=0.17, 0.3, 0.7, 1.4, and 2.7). The prepared catalysts were then applied to the production of light olefin (ethylene and propylene) through catalytic cracking of C_5 raffinate. The effect of phosphorous content on their hydrothermal stability was investigated. The acidity of C-ZSM5 catalysts significantly decreased after hydrothermal treatment caused by dealumination of C-ZSM5 catalyst during the hydrothermal treatment. On the other hand, phosphorous-modified XP/C-ZSM5 reserved extended amount of acid sites after hydrothermal treatment, because phosphorous introduced in C-ZSM5 catalyst inhibited the dealumination of the catalyst. Catalytic activity over phosphorous free C-ZSM5 catalyst significantly decreased after hydrothermal treatment, which was mainly due to the dealumination of the catalyst during the hydrothermal treatment. On the other hand, phosphorous containing XP/C-ZSM5 catalyst exhibited high resistance for hydrothermal treatment. All the hydrothermal treated catalysts exhibited better catalytic activities than C-ZSM5-St. catalyst. Conversion of C_5 raffinate and yield for light olefins showed volcano-shaped trend with respect to phosphorous content, and 0.3P/C-ZSM5-St. catalyst showed the best catalytic performance. This result indicates that optimal phosphorous content was required for maximum production of light olefins, and in turn, phosphorous modification of ZSM-5 was an effective method to enhance the hydrothermal stability of the catalyst.

A set of lanthanum-containing phosphorous-modified porous ZSM-5

catalysts (LaX-P/C-ZSM5) were prepared with a variation of La/Al atomic ratio (X=0.3, 0.7, 0.9, and 1.2) by an impregnation method to obtaining high yield for light olefin by suppressing secondary reaction between reactants. The prepared catalysts were applied to the production of light olefins (ethylene and propylene) through catalytic cracking of C_5 raffinate. The effect of lanthanum content on the physicochemical properties and catalytic activities was investigated. Acidity and basicity of LaX-P/C-ZSM5 catalysts were strongly influenced by lanthanum content. Acidity of LaX-P/C-ZSM5 catalysts decreased with increasing lanthanum content, while basicity of the catalysts increased with increasing lanthanum content. Catalytic performance of LaX-P/C-ZSM5 catalysts was strongly influenced by acid and base properties of the catalyst. Conversion of C_5 raffinate decreased with decreasing acidity of the catalyst and selectivity for light olefins increased with increasing basicity of the catalysts. Among the catalysts tested, La0.7-P/C-ZSM5 catalyst with moderate acidity and basicity exhibited the best catalytic performance in terms of yield for light olefins. Thus, an optimal lanthanum content of LaX-P/C-ZSM5 catalysts was required for maximum production of light olefins.

In summary, various modifications of ZSM-5 catalysts were carried out to obtaining high yield for light olefin from catalytic cracking of C_5 raffinate. The mesoporous feature of ZSM-5 catalysts enhance the diffusion rate of reactant leading to a superior catalytic performance. Phosphorous modification of ZSM-5 catalysts improve the hydrothermal stability by preventing segregation of the framework aluminum atoms. Furthermore, lanthanum containing ZSM-5 catalysts adjust acid-base properties of the

catalysts leading to a maximum production of light olefins. Therefore, it is concluded that textural property and acid-base property of the catalyst played a crucial role in determining the catalytic performance in the catalytic cracking of C_5 raffinate to light olefins.

Bibliography

[1] J.S. Plotkin, “The changing dynamics olefins supply/demand”, *Catal. Today* **106** (2005) 10.

[2] J. Lu, Z. Zhao, C. Xu, P. Zhang, A. Duan, “FeHZSM-5 molecular sieves - Highly active catalysts for catalytic cracking of isobutane to produce ethylene and propylene”, *Catal. Commun.* **7** (2006) 199.

[3] World Light Olefin Analysis, *CMAI (Chemical Market Associates, INC.)* report (2005).

[4] N. Rahimi, R. Karimzadeh, “Catalytic cracking of hydrocarbons over modified ZSM-5 zeolites to produce light olefins: A review”, *Appl. Catal. A: Gen.* **398** (2011) 1.

[5] T. Ren, M. Patel, K. Blok, “Olefins from conventional and heavy feedstocks: Energy use in steam cracking and alternative processes”, *Energy* **31** (2006) 425.

[6] Y. Wei, F. Chang, Y. He, S. Meng, Y. Yang, Y. Qi, L. Lu, P. Xie, Y. He, “Production of light olefins and aromatic hydrocarbons through catalytic cracking of naphtha at lowered temperature”, *Stud. Surf. Sci. Catal.* **158** (2005) 1223.

[7] Y. Yoshimura, N. Kijima, T. Hayakawa, K. Murata, K. Suzuki, F. Mizukami, K. Matano, T. Konishi, T. Oikawa, M. Saito, T. Shiojima, K. Shiozawa, K. Wakui, G. Sawada, K. Sato, S. Matsuo, N. Yamaoka, “Catalytic cracking of naphtha to light olefins”, *Catal. Surv. Jpn.* **4** (2000) 157.

[8] N. Rane, M. Kersbulck, R.A. van Santen, E.J.M. Hensen, “Cracking of n-heptane over Brønsted acid sites and Lewis acid Ga sites in ZSM-5 zeolite”, *Micropor. Mesopor. Mater.* **110** (2008) 279.

[9] G. Jiang, L. Zhang, Z. Zhao, X. Zhou, A. Duan, C. Xu, J. Gao, “Highly

effective P-modified HZSM-5 catalyst for the cracking of C_4 alkanes to produce light olefins", *Appl. Catal. A: Gen.* **340** (2008) 176.

[10] K. Kubo, H. Iida, S. Namba, A. Igarashi, "Selective formation of light olefin by n-heptane cracking over HZSM-5 at high temperatures", *Micropor. Mesopor. Mater.* **149** (2012) 126.

[11] W.F. Pansing, "The catalytic cracking of hexadecane - Effects of impurities, olefins, and steam", *J. Phys. Chem.* **69** (1965) 392.

[12] J.C. Mol, "Industrial applications of olefin metathesis", *J. Mol. Catal. A: Chem* **213** (2004) 39.

[13] C. van Schalkwyk, A. Spamer, D.J. Moodley, T. Dube, J. Reynhardt, J.M. Botha, "Application of a WO_3/SiO_2 catalyst in an industrial environment: part I", *Appl. Catal. A: Gen.* **255** (2003) 121.

[14] M. Stöcker, "Methanol-to-hydrocarbons: Catalytic materials and their behavior", *Micropor. Mesopor. Mater.* **29** (1999) 3.

[15] Z.-M. Cui, Q. Liu, W.-G. Song, L.-J. Wan, "Insights into the mechanism of methanol-to-olefin conversion at zeolites with systematically selected framework structures", *Angew. Chem. Int. Ed.* **45** (2006) 6512.

[16] M.-A. Djieugoue, A.M. Prakash, L. Kevan, "Cataltyic study of Methanol-to-Olefins conversion in four small-pore silicoaluminophosphate melecular sieves: Influence of the structural type, nickel incorporation, nickel location, and nickel concentration", *J. Phys. Chem. B* **104** (2000) 6452.

[17] E. Heracleous, M Machli, A.A. Lemonidou, L.A. Vasolos, "Oxidative dehydrogention of ethane and propane over vanadia and molybdena supported catalysts", *J. Mol. Catal. A: Chem.* **232** (2005) 29.

[18] O.V. Buyevskaya, D. Wolf, M. Baerns, "Ethylene and propene by oxidative dehydrogenation of ethane and propane: 'Performance of rare-earth oxide-based catalysts and development of redox-type catalytic materials by combinatorial methods'", *Catal. Today* **62** (2009) 91.

[19] O.A. Barias, A. Holmen, E.A. Blekkan, “Propane dehydrogenation over supported Pt and Pt–Sn catalysts: Catalyst preparation, characterization, and activity measurements”, *J. Catal.* **158** (1996) 1.

[20] J.H. Lunssford, “The catalytic oxidative coupling of methane”, *Angew. Chem. Int. Ed.* **34** (1995) 970.

[21] J.S. Lee, S.T. Oyama, “Oxidative coupling of methane to higher hydrocarbons”, *Catal. Rev. –Sci. Egn.* **30** (1988) 249.

[22] Q. Zhao, S.-L. Chen, J.Gao, C. Xu, “Effect of tungsten oxide loading on metathesis activity of ethane and 2-butene over WO_3/SiO_2 catalysts”, *Transition Met. Chem.* **34** (2009) 621.

[23] S.I. Kantorowicz, “C_4 processing options to upgrade steam cracker and FCC streams”, *Lecture presented at the Second Asian Petrochemicals Technology Conference*, 7–8 May (2002) Seoul, Korea.

[24] S. Huang, S. Liu, W. Xin. S. Xie, Q. Wang, L. Xu, “Effect of reaction temperature and pressure on the metathesis reaction between ethane and 2-butene to propene on the WO_3/Al_2O_3-HY catalyst”, *J. Nat. Gas Chem.* **15** (2006) 93.

[25] Z. Li, J. Martínez-Triguero, P. Concepción, J. Yub, A. Corma, “Methanol to olefins: activity and stability of nanosized SAPO-34 molecular sieves and control of selectivity by silicon distribution”, *Phys. Chem. Chem. Phys.* **15** (2013) 14670.

[26] M. Bjørgen, F. Joensen, M.S. Holm, U. Olsbye, K.-P. Lillerud, S. Sve, “Methanol to gasoline over zeolite H-ZSM-5: Improved catalyst performance by treatment with NaOH”, *Appl. Catal. A: Gen.* **345** (2008) 43.

[27] M. Firoozi, M. Baghalha, M. Asadi, “The effect of micro and nano particle sizes of H-ZSM-5 on the selectivity of MTP reaction”, *Catal. Commun.* **10** (2009) 1582.

[28] O.V. Buyevskaya, M. Baerns, “Catalytic selective oxidation of propane”, *Catal. Today* **42** (1998) 315.

[29] D.L. Stern, R.K. Grasselli, “Mechanistic aspects of propane oxidation over Ni-Co-molybdate catalysts”, *Stud. Surf. Sci. Catal.* **110** (1997) 357.

[30] D. Levin, J.Y. Ying, “Oxidative dehydrogenation of propane by non-stoichiometric nickel molybdates”, *Stud. Surf. Sci. Catal.* **110** (1997) 367.

[31] T. Ito, J. Wang, C.-H. Lin, J.H. Lunsford, “Oxidative dimerization of methane over a lithium-promoted magnesium oxide catalyst”, *J. Am. Chem. Soc.* **107** (1985) 5062.

[32] C.T. Au, K.D. Chen, C.F. Ng, “The modification of Gd_2O_3 with BaO for the oxidative coupling of methane reactions”, *Appl. Catal. A: Gen.* **170** (1998) 81.

[33] A. Palermo, J.P.H. Vazquez, R.M. Lambert, “New efficient catalysts for the oxidative coupling of methane”, *Catal. Lett.* **68** (2001) 191.

[34] A.A. Lemonidou, I.A. Vasalos, E.J. Hirschberg , R.J. Bertolacini, “Catalyst evaluation and kinetic study for ethylene production”, *Ind. Eng. Chem. Res.* **28** (1989) 524.

[35] R. Mukhopadhyay, D. Kunzru, “Catalytic pyrolysis of naphtha on calcium aluminate catalysts. Effect of potassium carbonate impregnation”, *Ind. Eng. Chem. Res.* **32** (1993) 1914.

[36] B. Basu, D. Kunzru, “Catalytic pyrolysis of naphtha”, *Ind. Eng. Chem. Res.* **31** (1992) 146.

[37] A.D. Eastma, J.H. Kolts, “Oxidative dehydrogenation”, *U.S. Patent* (1983) 4,370,259.

[38] H.H. Kung, “Oxidative dehydrogenation of light (C_2 to C_4) alkanes”, *Adv. Catal.* **40** (1994) 1.

[39] F.C. Jentoft, B.C. Gates, “Solid-acid-catalyzed alkane cracking mechanisms: evidence from reactions of small probe molecules”, *Top. Catal.* **4** (1997) 1.

[40] K. Wakui, K. Satoh, G. Sawada, K. Shiozawa, K. Matano, K. Suzuki, T. Hayakawa, Y. Yoshimura, K. Murata, F. Mizukami, “Dehydrogenative cracking of n-butane using double-stage reaction”, *Appl. Catal. A: Gen.* **230** (2002) 195.

[41] X. Feng, G. Jiang, Z. Zhao, L. Wang, X. Li, A. Duan, J. Liu, C. Xu, J. Gao, “Highly effective F-modifed catalysts for the cracking of naphtha to produce light olefins”, *Energy Fuels* **24** (2010) 4111.

[42] B. Wang, Q. Gao, J. Gao, D. Ji, X. Wang, J. Suo, “Synthesis, charaterization and catalytic C_4 alkene cracking properties of zeolite ZSM-23”, *Appl. Catal. A: Gen.* **274** (2004) 167.

[43] G. Zhao, J. Teng, Y. Zhang, Z. Xie, Y. Yue, Q. Chen, Y. Tang, “Synthesis of ZSM-48 zeolites and their catalytic performance in C_4-olefin cracking reactions”, *Appl. Catal. A: Gen.* **299** (2006) 167.

[44] X. Zhu, S. Liu, Y. Song, S. Xie, L. Xu, “Catalytic cracking of 1-butene to propene and ethene on MCM-22 zeolite”, *Appl. Catal. A: Gen.* **290** (2005) 191.

[45] L. Díaz, E. Kokkoli, O.Terasaki, M. Tsapatsis, “Surface structure of zeolite (MFI) crystals”, *Chem. Mater.* **16** (2004) 5226.

[46] K.P. Dey, S. Ghosh, M.K. Naskar, “Organic template-free synthesis of ZSM-5 zeolite particles using rice husk ash as silica source”, *Ceram. Int.* **39** (2013) 2153.

[47] J. Schulz, F. Bandermann, “Conversion of ethanol over H-ZSM-5”, *Chem. Eng. Technol.* **17** (1994) 179.

[48] S. Liu, R. Ohnishi, M. Ichikawa, “Promotional role of water added to methane feed on catalytic performance in the methane dehydroaromatization reaction on Mo/HZSM-5 catalyst”, *J. Catal.* **220** (2003) 57.

[49] R.L. Van Mao, L.H. Dao, “Ethylene light olefins from ethanol”, *U.S. Patent* 4,698,452 (1987).

[50] J. Zhuang, D. Ma, G. Yang, Z. Yan, X. Liu, X. Liu, X. Han, X. Bao, P. Xie, Z. Liu, “Solid-state MAS NMR studies on the hydrothermal stability of the zeolite catalysts for residual oil selective catalytic cracking”, *J. Catal.* **228** (2004) 234.

[51] G. Lischke, R. Eckelt, H.-G. Jerschkewitz, B. Parlitz, E. Schreier, W. Storek, B. Zibrowius, G. Öhlmann, “Spectroscopic and physicochemical characterization of P-Modified H-ZSM-5”, *J. Catal.* **132** (1991) 229.

[52] W. Song, R.E. Justice, C.A. Jones, V.H. Grassian, S.C. Larsen, “Synthesis, characterization, and adsorption properties of nanocrystalline ZSM-5”, *Langmuir* **20** (2004) 8301.

[53] J.C. Groen, J.C. Jansen, J.A. Moulijn, J. Pérez-Ramírez, “Optimal aluminum-assisted mesoporosity development in MFI zeolites by desilication”, *J. Phys. Chem. B* **108** (2004) 13062.

[54] M. Ogura, S.H. Shinomiya, J. Tateno, Y. Nara, E. Kikuchi, M. Matsukata, “Formation of uniform mesopores in ZSM-5 zeolite through treatment in alkaline solution” *Chem. Lett.* (2000) 882.

[55] S.-S. Kim, J. Shah, T.J. Pinnavaia, “Colloid-imprinted carbons as templates for the nanocasting synthesis of mesoporous ZSM-5 zeolite”, *Chem. Mater.* **15** (2003) 1664.

[56] C.H. Christensen, K. Johannsen, E. Törnqvist, I. Schmidt, H. Topsøe, C.H. Christensen, “Mesoporous zeolite single crystal catalysts: Diffusion and catalysis in hierarchical zeolites”, *Catal. Today* **128** (2007) 117.

[57] A.H. Janssen, I. Schmidt, C.J.H. Jacobsen, A.J. Koster, K.P. de Jong, “Exploratory study of mesopore templating with carbon during zeolite synthesis”, *Micropor. Mesopor. Mater.* **65** (2003) 59.

[58] Y. Tao, Y. Hattori, A. Matumoto, H. Kanoh, K. Kaneko, “Comparative study on pore structure of mesoporous ZSM-5 from resorcino-formaldehyde aerogel and carbon aerogel templating”, *J. Phys. Chem. B* **109** (2005) 194.

[59] C.H. Christensen, I. Schmidt, C.H. Christensen, “Improved performance of mesoporous zeolite single crystals in catalytic cracking and isomerization of n-hexadecane”, *Catal. Commun.* **5** (2004) 543.

[60] C.H. Christensen, K. Johannsen, I. Schmidt, C.H. Christensen, “Catalytic benzene alkylation over mesoporous zeolite single crystals: Improving activity and selectivity with a new family of porous materials”, *J. Am. Chem. Soc.* **125** (2003) 13370.

[61] M.Y. Kustova, S.B. Rasmussen, A.L. Kustov, C.H. Christensen, “Direct NO decomposition over conventional and mesoporous Cu-ZSM-5 and Cu-ZSM-11 catalysts: Improved performance with hierarchical zeolites”, *Appl. Catal. B: Environ.* **67** (2006) 60.

[62] H. Tao, C. Li, J. Ren, Y. Wang, G. Lu, “Synthesis of mesoporous zeolite single crystals with cheap porogens”, *J. Solid State Chem.* **184** (2011) 1820.

[63] E.L. Wu, S.L. Lawton, D.H. Olson, A.C. Rohrman, G. T. Kokotailo, “ZSM-5-type materials. Factors affecting crystal symmetry”, *J. Phys. Chem.* **83** (1979) 2777.

[64] L. Wang, Z. Zhang, C. Yin, Z. Shan, F.-S. Xiao, “Hierarchical mesoporous zeolites with controllable mesoporosity templated from cationic polymers”, *Micropor. Mesopor. Mater.* **131** (2010) 58.

[65] Y. Tao, H. Kanoh, K. Kaneko, “ZSM-5 monolith of uniform mesoporous channels”, *J. Am. Chem. Soc.* **125** (2003) 6044.

[66] G.D. Chen, L. Jiang, L.Z. Wang, J.L. Zhang, “Synthesis of mesoporous ZSM-5 by one-pot method in the presence of polyethylene glycol”, *Micropor. Mesopor. Mater.* **134** (2010) 189.

[67] O. Bortnovsky, P. Sazama, B. Wichterlova, “Cracking of pentenes to C_2-C_4 light olefins over zeolites and zeotypes: Role of topology and acid site strength and concentration”, *Appl. Catal. A: Gen.* **287** (2005) 203.

[68] R. Valiullin, J. Kärger, K. Cho, M. Choi, R. Ryoo, “Dynamics of water

diffusion in mesoporous zeolites", *Micropor. Mesopor. Mater*. **142** (2011) 236.

[69] K. Cho, H.S. Cho, L.-C. de Menorval, R. Ryoo, "Generation of mesoporosity in LTA zeolites by organosilane surfactant for rapid molecular transport in catalytic application", *Chem. Mater.* **21** (2009) 5664.

[70] J.S. Jung, J.W. Park, G. Seo, "Catalytic cracking of n-octane over alkali-treated MFI zeolite", *Appl. Catal. A: Gen.* **288** (2005) 149.

[71] V. Dondur, V. Raki, L. Damjanovi, R. Hercigonja, A. Auroux, "Temperature programmed desorption of n-hexane from hydrated HZSM-5 and NH_4ZSM5 zeolites", *J. Therm. Anal. Calorim.* **84** (2006) 233.

[72] W.J. van Well, J.P. Wolthuizen, B. Smit, J.H.C. van Hooff, R.A. van Santen, "Commensurate freezing n-alkanes in silicalite", *Angew. Chem. Int. Ed.* **34** (1995) 2543.

[73] B.A. Williams, S.M. Babitz, J.T. Miller, R.Q. Snurr, H.H. Kung, "The roles of acid strength and pore diffusion in the enhanced cracking activity of steamed Y zeolites", *Appl. Catal. A: Gen.* **177** (1999) 161.

[74] T. Blasco, A. Corma, J. Martínez-Triguero, "Hydrothermal stabilization of ZSM-5 catalytic-cracking additives by phosphorus addition", *J. Catal.* **237** (2006) 267.

[75] M.B. Sayed, R.A. Kydd, R.P. Cooney, "A Fourier-transform infrared spectral study of H-ZSM-5 surface sites and reactivity sequences in methanol conversion", *J. Catal.* **88** (1984) 137.

[76] F. Deng, Y. Du, C. Ye, J. Wang, T. Ding, H. Li, "Acid sites and hydration behavior of dealuminated zeolite HZSM-5: A high-resolution solid state NMR study", *J. Phys. Chem.* **99** (1995) 15208.

[77] A.P. Kentgens, M.K. Scholl, W.S. Veeman, "Effect of hydration on the local symmetry around aluminum in ZSM-5 zeolites studied by

aluminum-27 nuclear magnetic resonance", *J. Phys. Chem*. **87** (1983) 4357.

[78] B. Li, S. Li, N. Li, H. Chen, W. Zhang, X. Bao, B. Lin, "Structure and acidity of Mo/ZSM-5 synthesized by solid state reaction for methane dehydrogenation and aromatization", *Micropor. Mesopor. Mater*. **88** (2006) 244.

[79] G. Wang, C. Xu, J. Gao, "Study of cracking FCC naphtha in a secondary riser of the FCC unit for maximum propylene production", *Fuel Process. Technol.* **89** (2008) 864.

[80] D. Mier, A.T. Aguayo, M. Gamero, A.G. Gayubo, J. Bilbao, "Kinetic modeling of n-butane cracking of HZSM-5 zeolite catalyst", *Ind. Eng. Chem. Res.* **49** (2010) 8415.

[81] D. Wallenstein, R.H. Harding, "The dependence of ZSM-5 additive performance on the hydrogen-transfer activity of the REUSY base catalyst in fluid catalytic cracking", *Appl. Catal. A: Gen.* **214** (2001) 11.

[82] A.F.H. Wielers, M. Vaarkamp, M.F.M. Post, "Relation between properties and performance of zeolites in paraffin cracking", *J. Catal.* **127** (1991) 51.

[83] X. Zhu, S. Liu, Y. Song, L. Xu, "Catalytic cracking of C_4 alkenes to propene and ethene: Influences of zeolites pore structures and Si/Al ratios", *Appl. Catal. A: Gen.* **288** (2005) 134.

[84] K. Wakui, K. Satoh, G. Sawada, K. Shiozawa, K. Mantano, K. Suzuki, T. Hayakawa, K. Murata, Y. Yoshimura, F. Mizukami, "Catalytic cracking of n-butane over rare earth - loaded HZSM-5 catalysts", *Stud. Surf. Sci. Catal.* **125** (1999) 449.

[85] X. Lin, Y. Fan, Z. Liu, G. Shi, H. Liu, X. Bao, "A novel method for enhancing on-stream stability of fluid catalytic cracking (FCC) gasoline hydro-upgrading catalyst: Post-treatment of HZSM-5 zeolite by combined steaming and citric acid leaching", *J. Catal.* **125** (2007) 185.

초 록

석유화학산업의 기초원료로 이용되고 있는 경질 올레핀(에틸렌 및 프로필렌)은 합성수지, 합성고무, 합성섬유 등과 같은 석유화학제품을 생산하기 위한 기초 원료로 이용되는 매우 중요한 물질이다. 현재 경질 올레핀은 나프타를 수증기 존재 하에서 열분해하여 에틸렌과 프로필렌을 선택적으로 추출하는 방법에 의해 얻어진다. 하지만 나프타 분해 공정은 800도 이상의 매우 높은 온도에서 반응이 진행됨에 따라 석유화학 산업에서 1년 동안 사용하는 전체 에너지의 40%를 사용할 정도로 매우 높은 에너지를 소모하고 있으며, 이와 더불어 다량의 이산화탄소를 배출함으로써 지구 온난화에도 큰 영향을 미치고 있다. 경질 올레핀 수요의 증가와 경질 올레핀 생산 효율을 높이기 위한 방법으로 산 촉매를 이용한 촉매 접촉 분해 공정이 주목을 받고 있다. 촉매 접촉 분해 공정은 기존의 나프타 분해공정에 비해 보다 온화한 반응 조건에서 반응이 진행됨에 따라 에너지 효율을 높일 수 있으며, 또한 최종적으로 얻어지는 경질 올레핀의 선택도를 촉매 및 공정 조건을 변화함으로써 조절할 수 있는 장점이 있는 것이 특징이다. 특히, 나프타 분해공정에서 부산물로 생산되는 C_5 라피네이트를 반응물로 하여 촉매 접촉 분해 공정을 통해 경질 올레핀을 제조할 경우 석유자원의 효율적, 친환경적 활용이라는 관점에서 그 잠재력과 파급효과가 매우 큰 기술이라고 할 수 있다.

대표적인 산 촉매인 ZSM-5 제올라이트는 우수한 산 특성과 특유의 구조로 인해 크래킹, 이성질화, MTO (Methanol to olefins) 등의 석유화학 공정에 촉매로 널리 이용되고 있다. 특히 ZSM-5

를 촉매 접촉 분해 공정에 적용할 경우 우수한 활성을 나타내는 것으로 알려져 있다. 하지만, ZSM-5는 1nm이하의 미세기공을 가지는 것이 특징이다. ZSM-5의 이러한 특징은 반응물의 확산 저하를 일으켜 반응활성을 저하시키는 요인이 될 수 있다. 또한, 고온 다습한 반응조건 하에서 ZSM-5가 장시간 노출 될 경우 탈알루미늄 현상에 의해 촉매 비활성화가 나타나게 된다. 따라서 본 연구에서는 ZSM-5를 다양한 방법에 의해 변형시킴으로써 ZSM-5가 가지는 단점을 보완함과 동시에, 이들을 C_5 라피네이트의 촉매 접촉 분해를 통한 경질 올레핀 제조 반응에 도입함으로써 우수한 활성을 가지는 ZSM-5 촉매를 제조하였다.

ZSM-5 촉매에 반응물의 분자확산을 향상시킬 목적으로 PAM (polyacrylamide)를 주형물질로 이용하여 미세 및 중형 기공특성을 가지는 촉매(PAM(X)-ZSM5)를 제조하였다. 비교를 위해 주형물질을 포함하지 않은 ZSM-5 촉매 또한 제조하였다. 제조된 촉매를 C_5 라피네이트의 촉매 접촉 분해를 통한 경질 올레핀 제조 반응에 도입하였다. 주형물질로 사용되는 PAM의 양에 따른 촉매의 물리·화학적 특성 및 반응활성 결과를 비교해 보았다. 질소 흡·탈착 실험을 통해 실제로 PAM을 주형물질로 사용하였을 경우 의도한 대로 중형 기공 특성을 가지는 것을 확인 할 수 있었으며, 반응 실험 결과 중형 기공 특성을 가지는 촉매에서 보다 우수한 반응활성을 보이는 것을 확인 할 수 있었다. 이로부터 ZSM-5 촉매에 중형기공 특성을 부여할 경우 반응물의 분자확산이 향상되어 반응활성이 높아지는 것을 알 수 있었다.

PAM을 주형물질로 사용하여 미세 및 중형 물질로 이용하였을 경우, PAM이 과량 주입되게 되면 ZSM-5 촉매의 결정 형성을

억제하기 때문에 촉매의 결정성 및 산특성을 약화시키게 된다. 따라서 PAM을 대체할 수 있는 주형물질로써 탄소를 주형물질로 하여 미세 및 중형기공 특성을 가지는 ZSM-5 촉매(C(X)-ZSM5)를 제조하였다. 촉매 제조에 사용되는 탄소의 양을 다양한 범위 내에서 조절하여 촉매를 제조하였으며, 제조된 촉매를 C_5 라피네이트의 촉매 접촉 분해 반응에 이용하였다. 반응물로 사용되는 C_5 라피네이트의 구성물질 중 하나인 펜탄을 이용하여 승온 탈착법에 의해 흡착 능력을 비교해본 결과 촉매의 중형기공 특성이 향상될수록 흡착 능력이 향상된다는 것을 알 수 있었으며, 실제로 C_5 라피네이트의 촉매 접촉 분해 반응 결과에서도 중형기공 특성이 향상될수록 보다 높은 반응 활성을 나타냈다. 이로부터 촉매의 중형기공특성이 향상될수록 반응물의 확산을 향상시켜 보다 높은 경질 올레핀 수율을 얻을 수 있다는 것을 알 수 있었다.

탄소를 주형물질로 이용하여 제조된 C-ZSM5 촉매의 수열안정성을 향상시키기 위해 인이 도입된 촉매(P/C-ZSM5)를 제조하였다. 다양한 양의 인이 도입된 촉매를 제조하고, 제조된 촉매를 C_5 라피네이트의 촉매 접촉 분해 반응에 이용하였다. 촉매의 수열안정성을 실험하기 위해 제조된 촉매를 700도에서 3시간 동안 스팀처리 하였다. 스팀 처리 전·후의 촉매 산 특성을 확인해본 결과 인이 도입되지 않은 촉매의 경우 스팀처리가 진행되는 동안 탈알루미늄 현상에 의해 산량이 크게 감소되는 것을 확인 할 수 있었던 반면, 인이 도입된 촉매의 경우 감소되는 산량이 비교적 작은 것으로 나타났다. 스팀처리된 촉매를 이용한 C_5 유분의 촉매 접촉 분해 반응실험 결과 인이 도입되지 않은 촉매에 비해서 인이 도입된 촉매에서 보다 높은 경질 올레핀 수율을 얻을 수 있었으며,

이는 인이 도입된 촉매에서 스팀 처리 후 산 특성이 보다 잘 보존되어 분해활성이 유지되었기 때문이다. 이 결과로부터 ZSM-5 촉매에 인을 일정량 도입할 경우 촉매의 수열안정성을 향상시킴으로써 경질 올레핀을 보다 효과적으로 제조할 수 있다는 것을 알 수 있었다.

반응 생성물 및 중간 생성물의 2차 반응을 통한 부산물의 생성을 억제하고 경질 올레핀의 생성을 향상시키기 위한 목적으로 인이 도입된 촉매(P/C-ZSM5)에 란타늄이 도입된 촉매(La-P/C-ZSM5)를 제조하였다. 제조된 촉매를 C_5 라피네이트의 촉매 접촉 분해를 통한 경질 올레핀 제조 반응이 적용하였다. 촉매에 도입되는 란타늄의 양을 조절 하여 도입된 란타늄의 양이 촉매의 물리·화학적 특성 및 반응활성에 미치는 영향에 대해 알아보았다. 특성분석 결과 도입된 란타늄의 양에 따라 촉매의 산·염기 특성이 크게 변화하는 것을 알 수 있었다. 반응실험 결과 촉매의 산량이 감소함에 따라 C_5 라피네이트의 전환율을 감소한 반면, 염기량이 증가함에 따라 경질 올레핀 선택도가 증가하는 경향을 보이면서 촉매의 란타늄 함량에 대해 경질 올레핀 수율을 화산형 분포의 경향을 나타내는 것을 알 수 있었다. 이로부터 촉매의 산·염기 특성이 C_5 라피네이트의 촉매 접촉 분해 반응 활성에 큰 영향을 미친다는 것을 알 수 있었다.

본 연구에서는 다양한 방법에 의해 기존의 ZSM-5 촉매 보다 물리·화학적 특성이 개선된 촉매를 제조하고, 이를 C_5 라피네이트의 촉매 접촉 분해를 통한 경질 올레핀 제조 반응에 적용하였다. 다양한 특성 분석을 통해서 촉매의 표면 및 기공 특성, 수열 안정성 및 산·염기 특성이 반응활성을 결정짓는 중요한

인자라는 것을 확인하였다.

주요어: ZSM-5, 경질 올레핀, C_5 라피네이트, 산 특성, 염기 특성, 촉매 접촉 분해

학 번: 2011-30280